Quaternary Science Reviews 319 (2023) 108343

Contents lists available at ScienceDirect

Quaternary Science Reviews

journal homepage: www.elsevier.com/locate/quascirev

Holocene summer temperature reconstruction based on a chironomid record from Sierra Nevada, southern Spain

Gonzalo Jiménez-Moreno [a,*], Oliver Heiri [b], Antonio García-Alix [a], R. Scott Anderson [c], Francisco J. Jiménez-Espejo [d], Charo López-Blanco [a], Laura Jiménez [a], Carmen Pérez-Martínez [e], Marta Rodrigo-Gámiz [a], Alejandro López-Avilés [a], Jon Camuera [d]

[a] Department of Stratigraphy and Paleontology, University of Granada, 18002, Granada, Spain
[b] Geoecology, Department of Environmental Sciences, University of Basel, 4056, Basel, Switzerland
[c] School of Earth & Sustainability, Northern Arizona University, Flagstaff, 86011, AZ, USA
[d] Andalusian Earth Sciences Institute (IACT), Spanish Research Council – University of Granada (CSIC-UGR), 18100, Armilla, (Granada), Spain
[e] Department of Ecology, University of Granada, 18071, Granada, Spain

ARTICLE INFO

Handling Editor: P Rioual

Keywords:
Chironomids
Summer temperature
Holocene
Last glacial period
Sierra Nevada
Western Europe

ABSTRACT

Obtaining accurate temperature reconstructions from the past is crucial in understanding the consequences of changes in external climate forcings, such as orbital-scale insolation or multidecadal to centennial-scale variability on the climate system and the environment. In addition, these reconstructions help in comprehending the amplitude of natural temperature changes in the past, which can assist in evaluating the amplitude and rate of recent anthropogenic global warming. Here we present the first detailed Holocene mean July air temperature reconstruction based on chironomid assemblages from sediments retrieved from Laguna de Río Seco, an alpine lake in Sierra Nevada, southern Spain. Coldest climate conditions are recorded during the last glacial maximum and the last deglaciation. Warming occurred in the Early Holocene and warmest summer temperature conditions and the Holocene thermal maximum (HTM) occurred in the interval roughly between 9000 and 7200 cal yr BP, concurrent with summer insolation maxima. Rapid cooling of ~1.5 °C occurred after the warmest maximum and between ~7200 and 6500 cal yr BP, and temperatures stabilized between ~6500 and 3000 cal yr BP. A further cooling began ~3000 cal yr BP and culminated with coldest summer conditions during the Dark Ages (DA) and Little Ice Age (LIA) at ~1550 cal yr BP (~400 CE) and ~200 cal yr BP (~1750 CE), respectively. This cooling temperature trend was interrupted by warmer conditions during the Iberian-Roman Humid Period (IRHP) ~2000 cal yr BP and during the Medieval Climate Anomaly (MCA) at ~1000 cal yr BP. Our reconstruction shows a greater than two-degree cooling during the Middle and Late Holocene, agreeing with global mean surface temperature (GMST) reconstructions. Modern climate warming (MCW) during summer exceeds the two-degree Celsius forecasted for the future due to anthropogenic greenhouse gases, suggesting that recent warming is amplified at high elevations. Alpine environments and the biodiversity contained there are thus in danger if the observed temperature trend continues in the next decades.

1. Introduction

The Intergovernmental Panel on Climate Change (IPCC et al., 2022) predicts a possible increase in global temperatures of ~2 °C (higher than the period 1850–1900 CE) by the end of the 21st century. Impacts of increasing temperatures in mountains have been documented in recent decades with observable and serious consequences for societies, biodiversity, and ecosystems. These include, for example, changing seasonal weather patterns, reductions in snow cover extent and duration at low elevation, loss of glacier mass, increased permafrost thaw, changes in the timing of glacier- and snow-melt discharge, enhanced fire activity, and changing natural distribution of plant and animal species shifting to higher elevations (IPCC et al., 2022). Previous studies show that warming will be more pronounced in high altitude alpine areas (Pepin et al., 2022) causing dramatic impacts to those environments. Some areas of southern Europe are the most responsive regions to MCW,

* Corresponding author.
E-mail address: gonzaloj@ugr.es (G. Jiménez-Moreno).

https://doi.org/10.1016/j.quascirev.2023.108343
Received 23 July 2023; Received in revised form 25 September 2023; Accepted 26 September 2023
Available online 29 September 2023

especially in summer (Lorenzo and Alvarez, 2022). In addition, the Mediterranean side of southern Iberia appears to be especially sensitive as the occurrence of summer heatwaves has increased by 4% per decade between 1950 and 2020 CE (Díaz-Poso et al., 2023).

Understanding the long-term relationship between environmental change caused by climate change in mountain areas from the Mediterranean basin is paramount to comprehend ecosystem response to increasing temperatures in this climate-sensitive area. To accomplish this, detailed paleoecological and paleoclimatic studies are necessary, especially for periods that are warmer than present. In this respect, the sedimentary record from the alpine lake Laguna de Río Seco (LdRS; Fig. 1) has already provided detailed insights into environmental change in the Sierra Nevada range of southern Spain and the western Mediterranean area in general (sedimentation, eolian input, vegetation and lake environmental geochemistry) including information on past climate variations and human impact during the Holocene (~last 12,000 years; Anderson et al., 2011; García-Alix et al., 2013, 2018, 2020; Jiménez-Espejo et al., 2014; Jiménez et al., 2018, 2019; Toney et al., 2020). However, most of these previous paleoenvironmental studies were only interpreted in terms of qualitative paleoclimatic change and the only available temperature reconstruction comes from algae-derived long-chain diol analysis (García-Alix et al., 2020; Toney et al., 2020). Accurate quantitative temperature reconstructions are crucial to calibrate responses of the climate system to external forcing such as orbital-scale changes in insolation or multidecadal to centennial-scale climate variability and to help modelers parameterize their climate projections under different scenarios in the past, thereby contributing to more accurate climate predictions for the future (e.g., Heiri et al., 2014; PAGES 2k-PMIP3 group, 2015; Samartin et al., 2017).

Here we show a detailed fossil chironomid analysis of the Laguna de Río Seco record (LdRS-01, covering the past ~21,000 cal yr BP; Fig. 2). Remains of chironomid larvae, mainly their chitinous head capsules, are preserved well in Pleistocene and Holocene lake sediments (Bolland et al., 2020, 2021; Bennike et al., 2023). The head capsules of the different species possess unique morphological characteristics permitting their identification at the generic, species-group, or morphotype levels (Brooks et al., 2007). Chironomid assemblages are known to be sensitive to summer temperatures in continental environments (Brooks, 2006; Eggermont and Heiri, 2012) and can be used to estimate past summer temperature variability based on changes in species assemblages (e.g., Brooks and Birks, 2001; Samartin et al., 2017). The LdRS-01 chironomid record, therefore, allows the development of a quantitative summer temperature reconstruction for the Sierra Nevada region since the end of the Last Glacial Maximum (LGM). The comparison of this summer temperature record with other paleoclimate records will help refine our understanding of regional climate dynamics during the deglaciation and the Holocene, the extent that recent climate warming exceeds this baseline variability, and the impacts of climatic change on the environment in a mountain area in southern Spain.

2. Study site and regional setting

LdRS (37°03′7″N, 3°20′44″W, 3029 m a.s.l.) is in a south-facing glacial cirque basin located in the Sierra Nevada range, southern Spain (Fig. 1). The lake has a maximum depth of ~3 m, a surface area of 0.42 ha, and a drainage basin of 9.9 ha (Morales-Baquero et al., 1999).

Climate in the area is Mediterranean, with hot and dry summers. Meteorological records at 2500 m a.s.l. show mean annual temperature of ~4.4 °C, ranging from ~18 °C in summer to ~ −4 °C in winter. The annual precipitation at this elevation is between ~700 and 750 mm and mainly falls as snow between October and May (Observatorio del cambio global de Sierra Nevada, 2020; Spanish National Weather Agency –

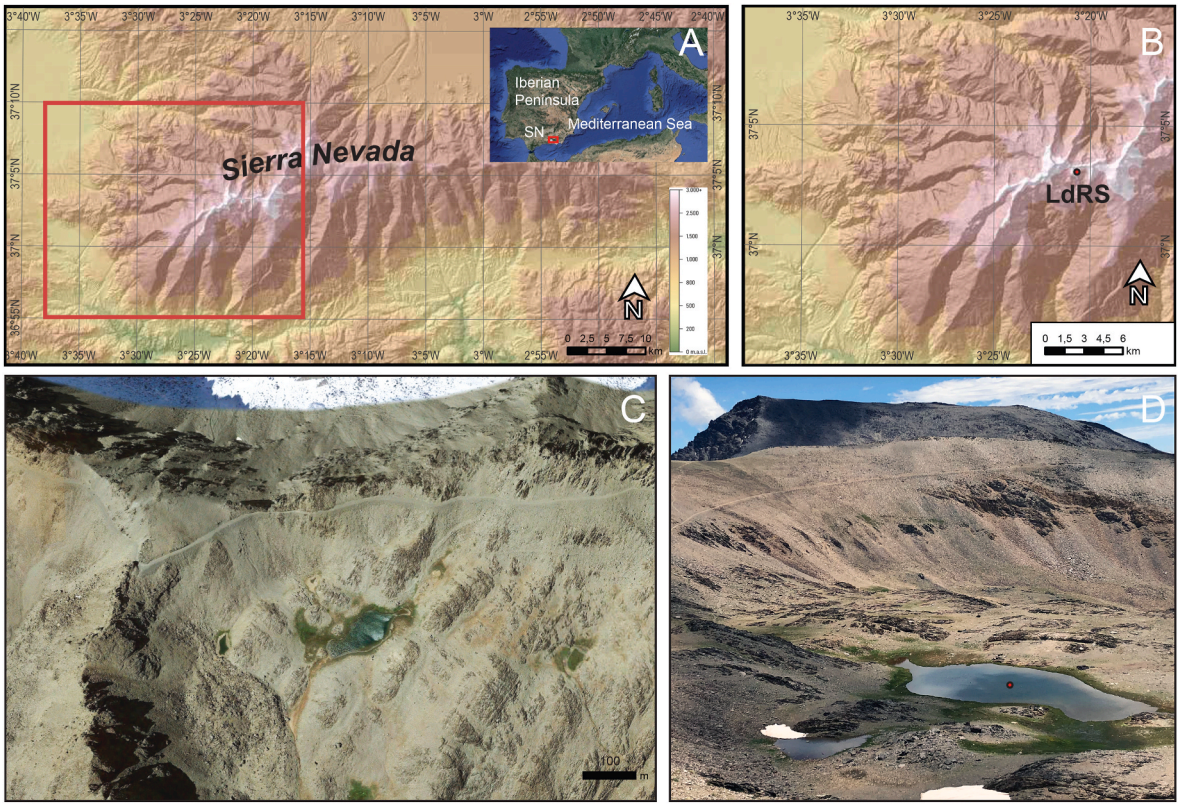

Fig. 1. Location (A and B) and photos (C and D) of LdRS in Sierra Nevada, southern Spain. (A) Map of the Sierra Nevada (SN in A) mountain range, southern Iberian Peninsula (modified from Jiménez-Moreno et al., 2022). The rectangle shows the magnified area shown in (B). (C) Satellite photo of the LdRS area from Google Earth. (D) Field photo of LdRS with the location of the core taken in September 2006. The Mulhacén, the highest peak in the Iberian Peninsula with 3479 m a.s.l., is in the background.

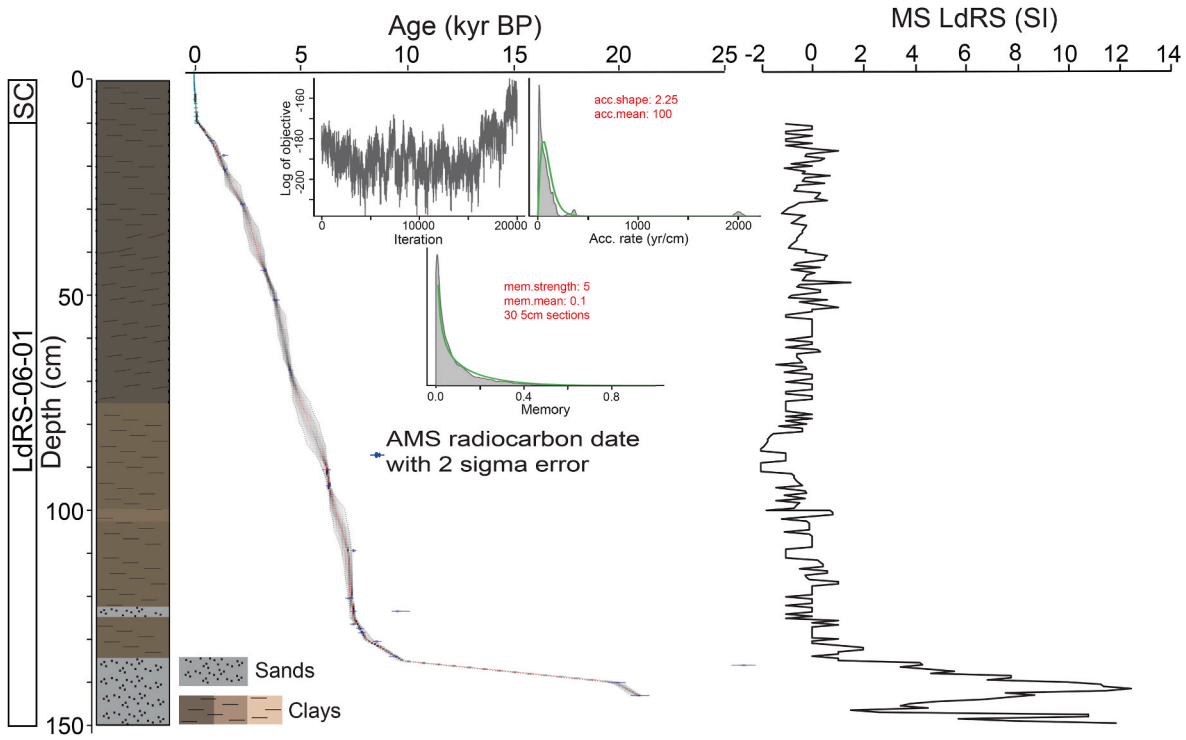

Fig. 2. Lithology, Bayesian age-depth model, and MS for the LdRS record. Lithology and MS were previously described in Anderson et al. (2011). On the left, SC stands for short core RS recovered in 2008 (see details in Jiménez et al., 2019). Blue areas in the age-depth model represent the calibrated radiocarbon ages along with their uncertainties, the red line indicates the weighted median ages and the dotted line around the grey shaded area shows the 95% confidence interval of the modelled ages. The different parameters and priors of the model are explained in the text.

AEMet Open Data, 2022). The LdRS lake water temperature has been monitored since 2011 and oscillates between ~0 °C in February–March and ~16 °C in July–August, with a mean temperature in July of 14.7 °C and a mean temperature for the summer months (June-July-August) of 12 °C. Surface air temperatures around LdRS have been measured from 2019 to 2022 and range from −5 to 15 °C, with a mean annual air temperature of 2.7 °C, mean July temperature of 14 °C and a mean temperature for the summer months of 13 °C.

LdRS is meso-oligotrophic (TP = 16 μg/L, TN = 403 μg/L; Chlorophyll: ~0.5-2 μ g/L) (Jiménez et al., 2019; Morales-Baquero and Conde-Porcuna, 2000) and its very narrow shoreline is covered by bryophytes. It has intermittent water inflows, providing water to the lake during late spring and early summer, and a small outlet that is only active during the highest lake water level (in June–July). The lake is covered in ice and snow from around October–November until May–June, depending on the year. The pH values range from 6 to 7.4, conductivity does not exceed 80 μS/cm, and the dissolved organic carbon values range from 0.74 to 3.40 mg/L. It does not thermally stratify (see thermistor data in García-Jurado et al., 2011) so the bottom is highly oxygenated, and during the ice-free period, Secchi disk visibility exceeds the water depth. It is a fishless lake with low planktonic diversity (Jiménez et al., 2019). More detailed limnological data are compiled by e.g. Sánchez-Castillo et al. (1989), Morales-Baquero et al. (1999) and Reche et al. (2005).

LdRS (37°03′N, 3°20′W) is situated above the treeline (above ~2500 m a.s.l.), where extreme climate conditions occur. Vegetation in these alpine environments is typically cryoromediterranean, characterized by tundra-like open grassland and plants with basal rosettes (Valle, 2003; Anderson et al., 2011). The LdRS catchment area is partially vegetated (~15%) by alpine meadows, primarily made up of sedges (Cyperaceae) and grasses (Poaceae), and xerophytic shrubland (Anderson et al., 2011). The rest of the catchment area is characterized by bare rocks that like the lake bedrock are mainly composed of mica schists (Díaz de Federico, 1980).

3. Materials and methods

Two adjacent sediment cores were collected in September 2006 at the depocenter of LdRS from a floating platform anchored to the shore. These included a 150 cm-long core (LdRS-06-01) using a Livingstone square-rod piston corer, and a 37 cm-long core (LdRS-06-02) using a universal corer with a plexiglass tube (Aquatic Research, Inc.) to recover the unconsolidated upper sediments. Maximum depth of the lake when cored was 1.7 m.

Sediment characteristics for both cores were described in the laboratory (see Anderson et al., 2011 for more details; Fig. 2). Magnetic susceptibility (MS) for LdRS-06-01 was determined using a Bartington MS2E meter with measurements taken every 5 mm throughout the length of the core (Fig. 2). MS was not done on core LdRS-06-02 as the sediments were sampled in the field and were put in whirlpack bags. Nine bulk sediment samples in the LdRS-06-01 core were previously analyzed for radiocarbon dating and 11 samples from the upper 16 cm of core LdRS-06-02 were previously analyzed for ^{210}Pb and ^{137}Cs dating (Anderson et al., 2011). In this study, a further batch of twelve bulk sediment samples were taken from the lowermost and uppermost parts of the LdRS-06-01 core for radiocarbon analysis (Table 1; Fig. 2). All the results from radiocarbon analyses (21 radiocarbon dates in total) were converted to calibrated radiocarbon years before present (cal yr BP, with present taken at 1950 CE by convention) using the IntCal20 calibration curve (Reimer et al., 2020) and a revised Bayesian age-model has been calculated using the R-based Bacon package, version 3.1.0 (Blaauw and Christen, 2011, Fig. 2). Two seemingly old samples (in red in Table 1) were not included in the age-depth model. The age-depth model that provided the lowest uncertainties was obtained by computing Markov Chain Monte Carlo (MCMC) interrelations in 30 sections of 5 cm with the accumulation priors 2.25 (shape) and 100 (mean). Low values were set for the memory priors (memory strength = 5 and memory mean = 0.1) due to the large shifts in the accumulation rates at the top and at the bottom of the core (Fig. 2).

Table 1
Radiometric ages from Laguna de Río Seco cores 06-01 and 06-02. In bold the twelve new radiocarbon analyses carried out in this study. In red the dates that were rejected for the age model construction. Radiocarbon ages were calibrated using the IntCal 20 calibration curve (Reimer et al., 2020).

Laboratory Code	Core	Real depth (cm)	14C age (yr BP)	SD (±)	Calibrated Age (cal yr BP)
Surface	Surface	0		5	-56
	LdRS 06-02	4.5	137Cs	10	-13
	LdRS 06-02	10	210Pb	30	74
BETA656622	**LdRS 06-01**	**14.6**	**870**	**30**	**765**
BETA 656623	**LdRS 06-01**	**18**	**1480**	**30**	**1357**
UCIAMS 51255	LdRS 06-01	21.2	1520	15	1398
UCIAMS 63003	LdRS 06-01	29.3	2255	20	2234
UCIAMS 51256	LdRS 06-01	44.6	3060	15	3295
UCIAMS 63004	LdRS 06-01	51.5	3525	20	3786
UCIAMS 51257	LdRS 06-01	67.7	4010	15	4480
UCIAMS 51258	LdRS 06-01	90.8	5450	30	6246
UCIAMS 63005	LdRS 06-01	94.5	5505	20	6298
UCIAMS 63006	LdRS 06-01	109.5	6550	20	7453
BETA 645325	**LdRS 06-01**	**120.5**	**6360**	**30**	**7284**
BETA 650528	**LdRS 06-01**	**123.5**	**6560**	**30**	**7465**
UCIAMS 32495	LdRS 06-01	123.5	8570	60	9540
BETA 645326	**LdRS 06-01**	**126.5**	**6550**	**30**	**7461**
BETA 645327	**LdRS 06-01**	**127.5**	**6930**	**30**	**7751**
BETA 645328	**LdRS 06-01**	**128.5**	**7060**	**30**	**7890**
BETA 632083	**LdRS 06-01**	**130.5**	**7770**	**30**	**8550**
BETA 650529	**LdRS 06-01**	**134**	**8450**	**40**	**9481**
BETA 645328	**LdRS 06-01**	**136**	**21550**	**80**	**25862**
BETA 632084	**LdRS 06-01**	**140**	**16430**	**60**	**19803**
BETA 632085	**LdRS 06-01**	**143**	**17360**	**50**	**20930**

Forty-eight samples of 2 cm^3 from core LdRS-06-01 were processed for chironomid analysis, which involved chemical treatment with sodium hexametaphosphate, sieving at 100-μm, sorting of chironomids from sieve residue at ca. 30x magnification, and identification of chironomids on slides with Euparal medium with a light-transmitted microscope at 100x - 400x magnification (Brooks et al., 2007). The taxonomical identifications mostly followed Brooks et al. (2007) (Fig. 3). These chironomid counts were combined with previously published chironomid data from ten samples from another short core taken from the depocenter of the LdRS basin, RS, covering 155 to −55 cal yr BP (Jiménez et al., 2019). This way, a composite chironomid record of chironomid assemblage change in LdRS was produced from two cores, LdRS-06-01 and RS, which were independently dated and were correlated by chronostratigraphy. Chironomid relative abundances (%) were calculated with respect to the total chironomid count in each sample and were plotted using TILIA (Grimm, 1992) in a detailed diagram shown in Fig. 4 where all the identified taxa are shown. A constrained incremental sum of squares cluster analysis (CONISS, Grimm, 1987) was performed to determine periods with similar chironomid assemblages (Fig. 4).

A Detrended correspondence analysis (DCA) was applied to the chironomid data to determine whether linear (PCA) or unimodal statistical (CA) techniques are the most appropriate to model the species response, estimated as units of compositional turnover in standard deviation (SD) of the first major gradient of the DCA. As the length of the exploratory DCA for the squared-root transformed data of chironomids was 2.5 SD, the assemblage variation is within a relatively narrow range and linear methods such as PCA are appropriate (Lepš and Šmilauer, 2003; Legendre and Birks, 2012). PCA was run on the chironomid percentage data using the Past4 software (Hammer et al., 2001). PCA determines variables (components) that represent, as much as possible, the variance of the multivariate data (Hammer et al., 2001). These new components are linear combinations of the original variables. The PCA can be used to summarize the data to, for example, only two variables (the first two components) for comparison in graphs. A PCA correlation loading and scatter biplot diagrams are shown in Fig. 5.

The most climate-sensitive indicators from chironomid (*Micropsectra radialis* type), pollen (*Artemisia*) and MS data are plotted together for visual comparison on Fig. 6.

Based on the fossil chironomid percentage data mean July air temperature estimations were produced using a 274-lake chironomid-temperature calibration dataset and transfer function from the Swiss Alps and Norway that covers a mean July air temperature gradient from 4 to 18.4 °C and a wide range of arctic, alpine, subalpine and temperate lakes (Heiri et al., 2011). This reconstruction was developed using the program C2 (Juggins, 2007) and the applied transfer function was based on weighted averaging partial least squares regression (WA-PLS; Ter Braak and Juggins, 1993; Ter Braak et al., 1993). The model featured a cross-validated r^2 of 0.9 and a root-mean-square error of prediction (RMSEP) of 1.39 °C. The RMSEP, coefficient of determination (R^2) and sample-specific errors of prediction (eSEPs) were calculated based on 9999 bootstrapping cycles in C2. Chironomid assemblage percentage data were square root transformed before the calculation of WA-PLS and distance metrics. A total of 19 sites with unusual hydrological or ecological conditions and high prediction residuals were deleted from the model as outliers as described in Heiri et al. (2011).

The quantitative summer (June-July-August) temperature from LdRS was also reconstructed using the pollen record (Anderson et al., 2011), which includes 69 fossil pollen samples from cores LdRS-06-01 and LdRS-06-02. In order to get an accurate reconstruction of a western European high-altitude mountain area, we used the Eurasian Modern Pollen Database v2 (EMPDv2) (Davis et al., 2020) delimited to latitude 25°-50°N and longitude 15°W-5°E, and excluding low-altitude (below 1500 m a.s.l.) modern pollen sites. The pollen taxonomy was harmonized using the Plants of the World online database (www.plantsoftheworldonline.org) and the Integrated Taxonomic Information System (www.itis.gov). Aquatic plants were removed, assuming that the distribution of these plants could be affected by other factors not related to climate. Therefore, the training set is based on 300 modern pollen sites and 194 harmonized pollen taxa. The recent temperature for each modern pollen site was obtained from the WorldClim v2.1 database under a 30 s resolution (www.worldclim.org) (Fick and Hijmans, 2017). The pollen-based transfer function from LdRS was developed using the C2 software under version 1.7.7 (Juggins, 2007). We used the two-component WA-PLS method under leave-one-out cross-validation. The WA-PLS method assumes that each taxon has a unimodal distribution with respect to climatic parameters and it is robust to spatial autocorrelation (Telford and Birks, 2005). The square-root species transformation was used to reduce the noise of the data. The WA-PLS of the summer temperature provided a leave-one-out, cross validated R^2 value of 0.71 and a RMSEP of 1.8 °C.

4. Results

4.1. New chronology for LdRS record

The twelve new radiocarbon analyses, together with the nine previous analyses, indicate that the LdRS-06-01 core contains a record of the past ~21,000 cal yr BP (Fig. 2; Table 1). The revised chronology shows that the LdRS sedimentary record is older than previously thought (~12,000 cal yr BP; Anderson et al., 2011), now dating back to at least the end of the LGM. This new chronology mostly concerns the

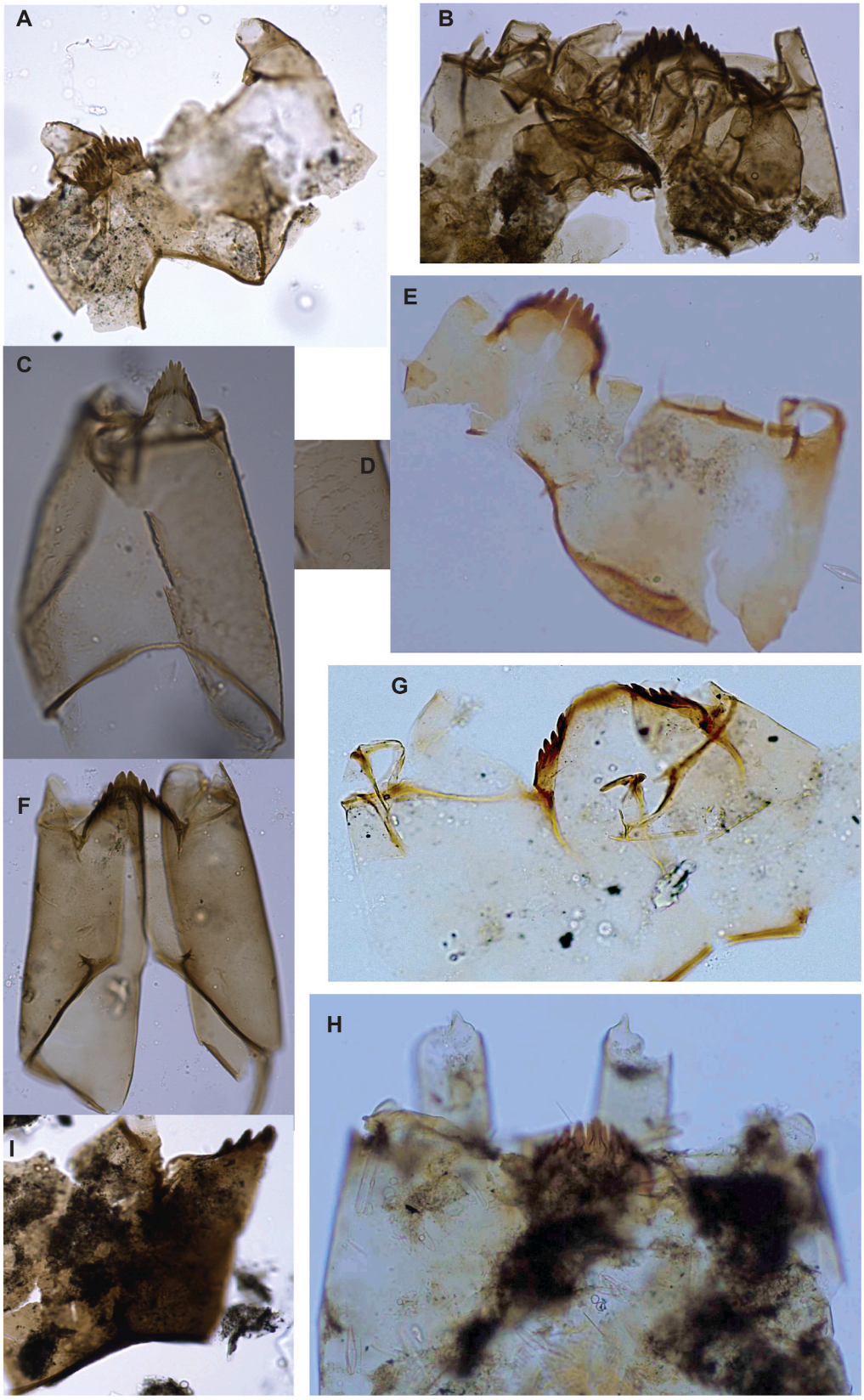

Fig. 3. Photos of chironomid remains from the LdRS sedimentary record: A - *Micropsectra radialis* type- LdRS Dr.03 10–11 cm; B - *Chironomus plumosus* type- LdRS Dr.02 10–11 cm; C - *Corynoneura arctica* type- LdRS Dr.01a 20–21 cm; D - *Corynoneura arctica* type LdRS Dr01a 20–21, head capsule surface ornamentation detail; E – *Metriocnemus*- LdRS Dr.01 64–65 cm; F - *Psectrocladius sordidellus* type LdRS Dr.01a 20–21 cm; *Psectrocladius* (*Alloseptrocladius*) *flavus* type- LdRS Dr.03 6–7 cm; *Micropsectra insignilobus* type- LdRS Dr.01 84–85 cm; *Heterotrissocladius marcidus* type- LdRS Dr.02 30–31 cm.

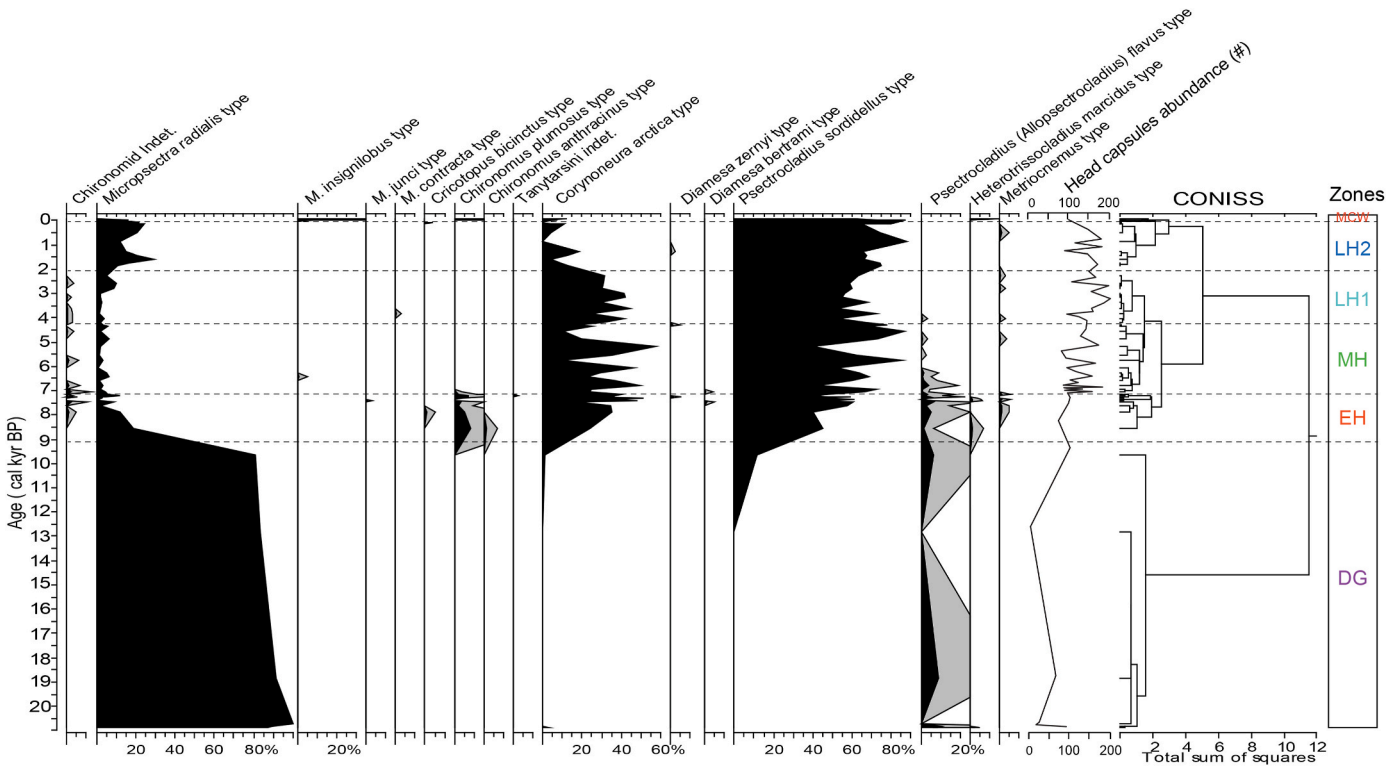

Fig. 4. Detailed diagram of chironomid assemblages changing over time in the LdRS record. Shadings show 5x exaggeration. On the right are the six chironomid zones identified using constrained incremental sum of squares (CONISS; Grimm, 1987) (see text for explanation).

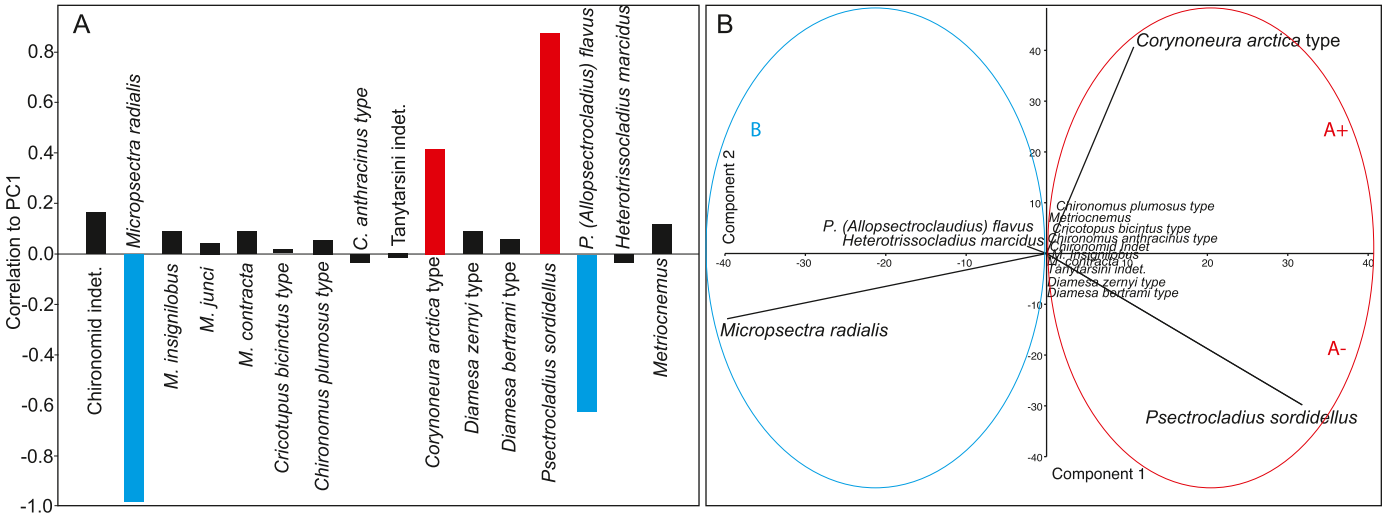

Fig. 5. Principal component analyses (PCA) from the LdRS chironomid data (A and B). A PCA correlation loading (to component 1) is shown in (A) and scatter biplot diagram is shown in (B). The analysis was carried out using PAST 4.10 (Hammer et al., 2001). Interpreted PCA groups are shown (see text for explanation).

bottommost part of the LdRS record, dilating the previous record from Early Holocene (EH) to the Latest Pleistocene age. The accumulation rate of the bottommost part of the record is very low 0.0007 cm/yr, contrasting with the mean sedimentation rate of the uppermost 135 cm (0.014 cm/yr). As the new radiocarbon datings for the bottommost part of the core are somehow ambiguous (25,862 yr BP at 136 cm, 19,803 yr BP at 140 cm and 20,930 yr BP at 143 cm), we use a conservative approach for the pre-Holocene section and used general terms as "Deglaciation *sensu lato*" or "Late Pleistocene" (see below).

4.2. Chironomid results

Fifteen morphotypes of chironomid taxa were identified in the composite chironomid record that consists of 48 analyzed samples from core LdRS-06-01 and 10 previously published chironomid samples from Jiménez et al. (2019). Chironomid concentrations in 2 cm^3 of sandy sediments from the bottommost part of the sedimentary record were low, with an average number of 50 identified head capsules, due to their very inorganic nature (Fig. 4). However, chironomid abundance increased considerably in the EH and remained high (average of 130) during the rest of the Holocene. Photographs of the most common and climatically significant taxa are shown in Fig. 3. Chironomid diversity in

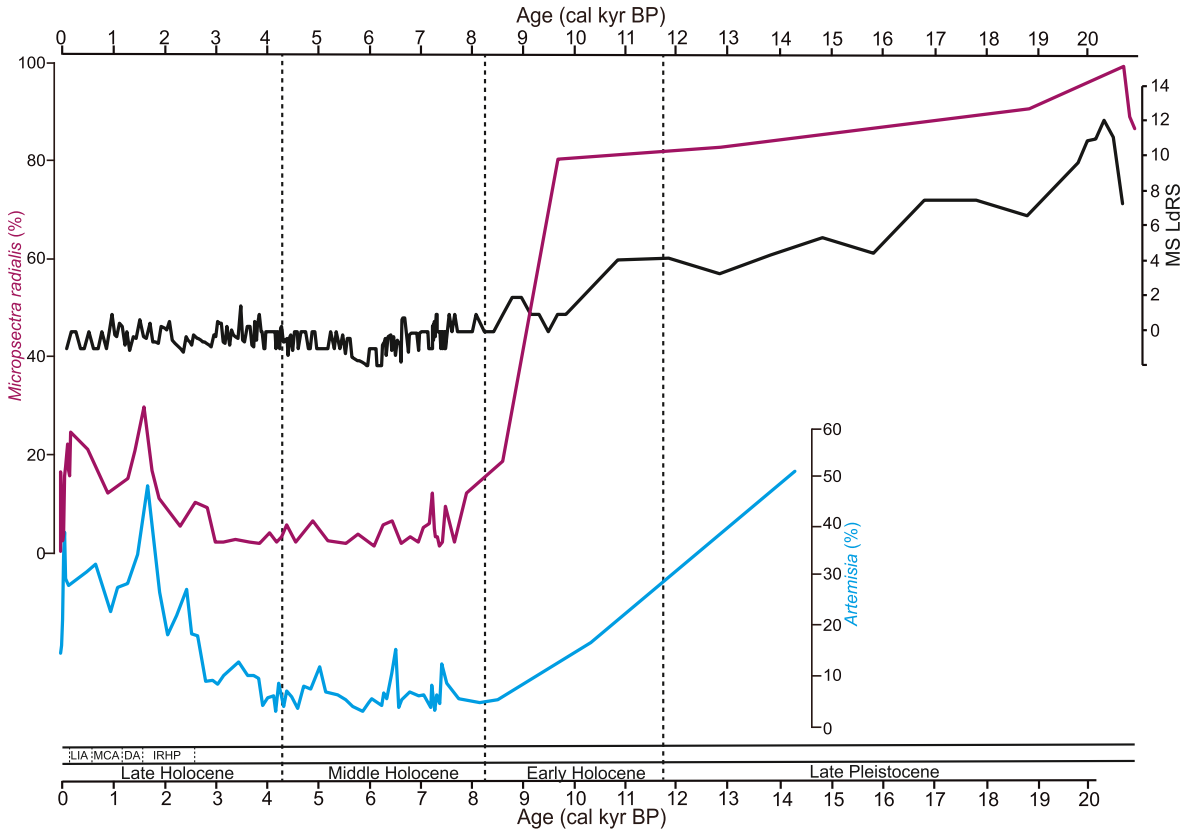

Fig. 6. Comparison of individual chironomid (*Micropsectra radialis* type), and pollen (*Artemisia*) taxa with sedimentation data (MS) from LdRS. MS and *Artemisia* data were previously published in Anderson et al. (2011). Note the visual covariation between the independent LdRS environmental indicators and chironomid data. Late Pleistocene and Early, Middle and Late Holocene boundaries are shown with dashed lines. IRHP, DA, MCA and LIA stand for Iberian Roman Humid Period, Dark Ages, Medieval Climate Anomaly and Little Ice Age.

the studied samples is relatively low, with 3–9 morphotypes per sample. *Micropsectra radialis* type, *Psectrocladius sordidellus* type and *Corynoneura arctica* type are the most abundant taxa in the sedimentary record (Figs. 3 and 4). Pronounced changes are observed in these and other taxa and with the help of the cluster analysis and visual observation we were able to distinguish the following periods (zones).

4.2.1. Deglaciation sensu lato (DG) - (146.5–132 cm; ~20,900–9000 cal yr BP)

The assemblages during this period including the latest Pleistocene and part of the EH are characterized by the abundance of *Micropsectra radialis* type, the dominant taxon with abundances between 80 and 100%, and *Psectrocladius (Allopsectrocladius) flavus* type.

4.2.2. Early Holocene sensu lato (EH) – (132-107 cm; ~9000-7100 cal yr BP)

Psectrocladius sordidellus type and *Corynoneura arctica* type appeared and increased during the EH and early MH, reaching around 50 and 40%, respectively. *Chironomus plumosus* type also appeared at the beginning of this period and disappeared at the end of it, showing average relative abundance of around 5%. *Micropsectra radialis* type decreased considerably to percentages lower than 5% and decreases of *Psectrocladius (Allopsectrocladius) flavus* type are also observed during this zone. *Chironomus anthracinus* type occurred at the beginning of this period. This period is also characterized by the occurrence of *Heterotrissocladius marcidus* type and *Metriocnemus* type, both reaching a maximum abundance of around 1%.

4.2.3. Middle Holocene (MH) - (107-59 cm; ~7100-4200 cal yr BP)

Psectrocladius sordidellus type displays an increasing trend during this period, reaching maxima higher than 85% at ~5800 and 4500 cal yr BP. *Corynoneura arctica* type seems to show a decreasing trend, with marked variability opposite to the abundances of *Psectrocladius sordidellus* type, and features minima at ~5800 and 4500 cal yr BP of around 12%. *Psectrocladius (Allopsectrocladius) flavus* type continued decreasing in this zone and disappeared at the end of it. *Micropsectra radialis* type occurred with percentages around 5% or lower in this period.

4.2.4. Late Holocene 1 (LH1) - (59-26 cm; ~4200-2000 cal yr BP)

Psectrocladius sordidellus type shows a decreasing trend at the beginning of this zone, reaching minima with percentages of 55% at 4000 and 3600 cal yr BP and an increasing trend at the end of the zone with values around 70%. *Corynoneura arctica* type shows the opposite trends, increasing first, reaching maxima (42%) around 3600 and 3100 cal yr BP and then decreasing down to 20% at the end of the period. *Micropsectra radialis* type increased at the end of this zone, reaching a peak of 10% between ~2700-2600 cal yr BP.

4.2.5. Late Holocene 2 (LH2) - (26–5.75 cm; ~2000-0 cal yr BP)

Psectrocladius sordidellus type depicts an increasing trend in this zone, reaching values above 85% at the end of it at ~900 and 0 cal yr BP. *Corynoneura arctica* type decreased considerably, reaching a minimum of almost 0% at ~900 and between 100 and 50 cal yr BP. *Micropsectra radialis* type continued increasing in this period to a peak of ~30% at ~1600 cal yr BP, subsequently decreased to ~12% at ~900 cal yr BP and increased again to 25% at the end of this zone at ~150 and 78 cal yr BP.

4.2.6. Modern climatic warming (MCW) - (5.75–0 cm; 0 to −58 cal yr BP; 1950–2008 CE)

The most noteworthy characteristic of this period consists of the renewed arrival of *Chironomus plumosus* type and *Heterotrissocladius marcidus* type, taxa that were previously abundant in the EH, as well as of *Micropsectra insignilobus* type (Fig. 4). *M. insignilobus* type increased in the past 50 years and reaches around 20% at present. *Heterotrissocladius marcidus* type and *Chironomus plumosus* type, which last occurred at ~8500 and 7000 cal yr BP in the LdRS record, respectively, reappeared again since 1970 CE.

4.3. PCA analysis of chironomid data

PCA indicates that principal component axis 1 (PC1) accounts for much of the variability of the data, explaining 73.5% of the variance. PC2 explains 24.9% of the variance. The PCA correlation loadings and scatter diagram shown in Fig. 5 illustrate to what degree the different taxa correlate with the different components. PCA shows two main groups of distinctive taxa (Fig. 5). One group (A), characterised by positive correlation to PC1, is mostly made up of *Corynoneura arctica* type and *Psectrocladius sordidellus* type but also by *Metriocnemus*, *Micropsectra insignilobus* type, *M. contracta* type and *Chironomus plumosus* type. A second group (B) is characterised by negative correlation values to PC1 and is mostly characterized by *Micropsectra radialis* type but also by *Psectrocladius (Allopsectrocladius) flavus* type. A subdivision of group A would be possible between taxa that show positive correlations to PC2 (A+), mostly characterized by *Corynoneura arctica* type, and taxa that show a negative correlation to PC2 (A-) dominated by *Psectrocladius sordidellus* type (Fig. 5B).

Cluster analysis of the chironomid data agrees with the PCA with chironomid zone DG characterized by high relative abundances of chironomids in the PCA B group (dominated by *Micropsectra radialis* type), zones EH, MH and LH1 by maxima of taxa belonging to the PCA A group, such as *Corynoneura arctica* type and *Psectrocladius sordidellus* type, with varying abundances of taxa in the A+ and A-groups. LH2 is characterized by an increase in chironomid taxa from PCA B group and MCW with higher abundances of those in the A group (Figs. 4 and 5).

4.4. Chironomid-inferred temperature results

Chironomid-inferred July air temperatures during zone DG oscillate between 4.5 and 7.5 °C (mean temperature around 6 °C), the lowest values in the record, and increase distinctly at the end of this period and onset of the Holocene (Fig. 7). The increasing temperature trend continues during the EH, reaching temperature maxima of 10.5–10.8 °C between ~8600 and 7200 cal yr BP. A minimum temperature of ~9.2 °C is recorded between those two maxima at ~7350 cal yr BP. Decreasing temperatures are observed during the beginning of the MH, reaching a plateau of around 9 °C between ~6500 and 3000 cal yr BP. Temperatures remained stable during the first part of LH1 until ~3000 cal yr BP when they decrease down to around 8.5 °C at ~2700 cal yr BP. A slight increase in temperatures to 9 °C occurs at the end of LH1 and the beginning of LH2 between ~2250 and 1800 cal yr BP. A decrease in temperatures occurs subsequently, recording a minimum below 8 °C at ~1550 cal yr BP. An increase occurs afterwards and a peak slightly above ~8 °C is observed at ~1200 cal yr BP (~700 CE) (Fig. 8). Temperatures decrease later on and a minimum around 8 °C is reached between ~1450-1800 and 1900 CE, separated by an increase to 8.5 °C at ~1850 CE. The chironomid-based air summer temperature reconstruction suggests an increasing trend from 1950 CE until the present reaching ~10.6 °C, one of the highest temperature values reached during the Holocene (Figs. 8 and 9).

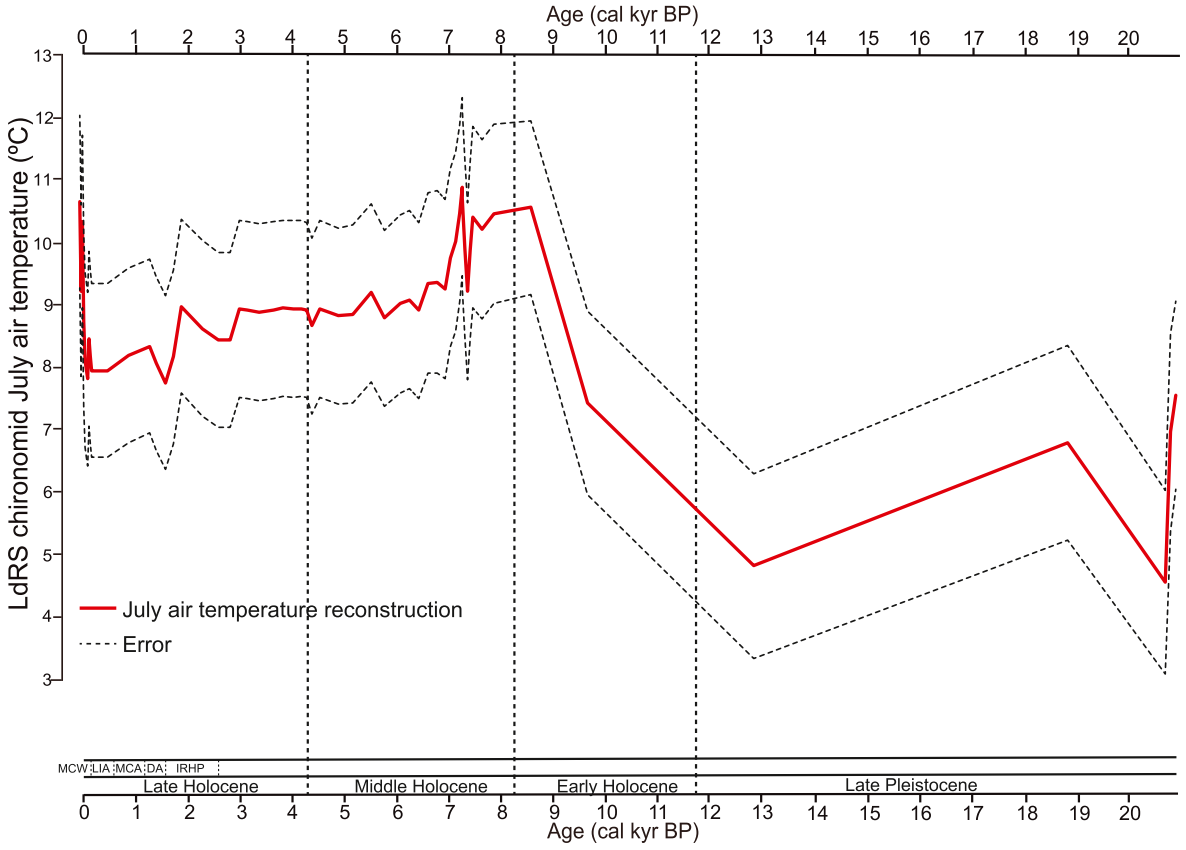

Fig. 7. Chironomid-inferred July air temperatures from the LdRS composite record (solid lines) and associated temperature estimate error (eSEP; dashed lines) for each sample. IRHP, DA, MCA, LIA and MCW stand for Iberian Roman Humid Period, Dark Ages, Medieval Climate Anomaly, Little Ice Age and Modern Climate Warming.

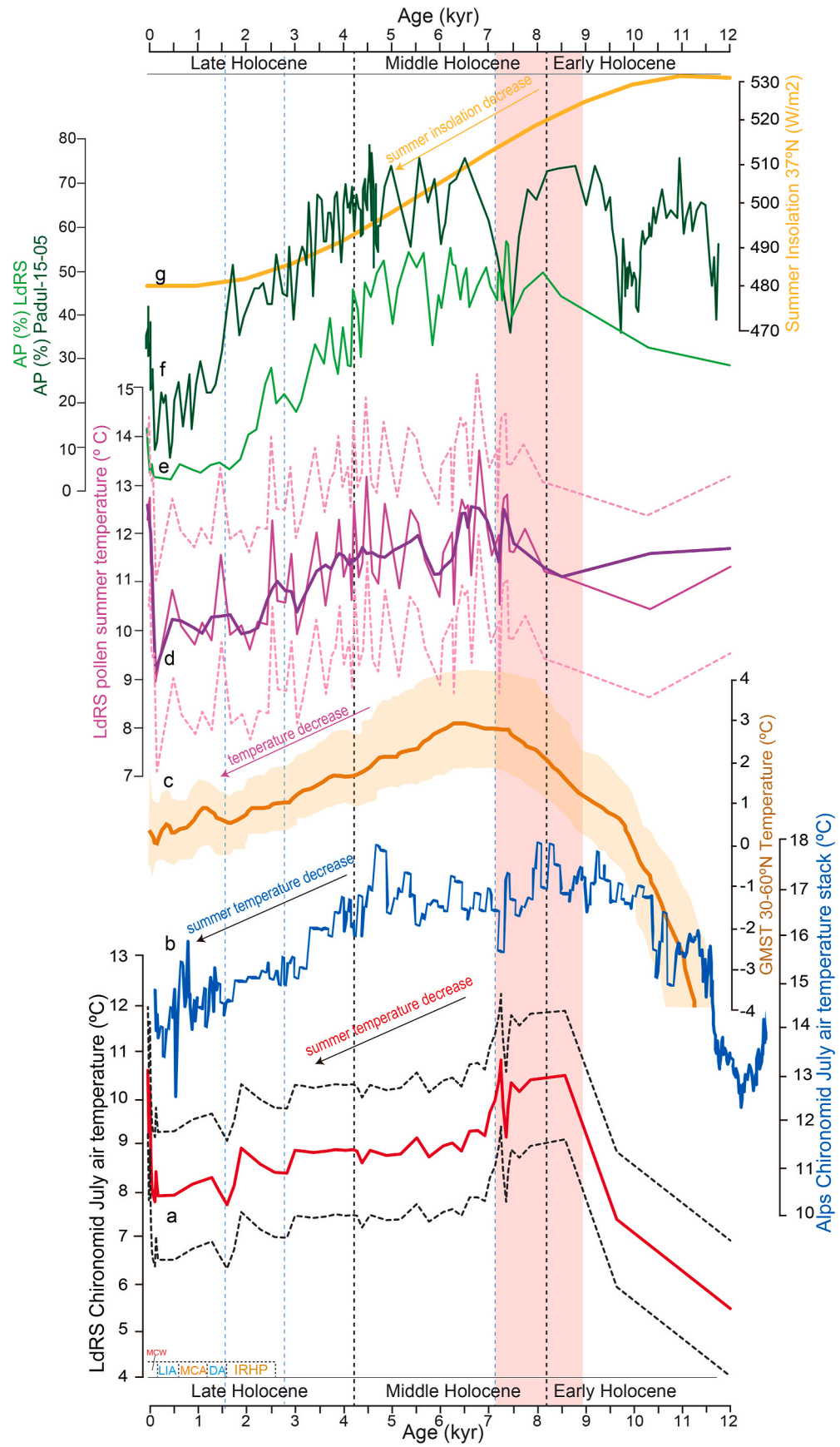

(caption on next page)

Fig. 8. Comparison of the chironomid-inferred July air temperature from LdRS (A) with (B) a stacked and spliced chironomid-based July air temperature reconstruction from the Alps (Heiri and Lotter, 2005), (C) global mean surface temperature (GMST) composite for 30-60°N (Kaufman et al., 2020a), (D) summer temperature reconstruction based on the pollen data from LdRS (thick purple line is a loess smoothing) and associated error estimates (dashed pink lines), (E) arboreal pollen (AP) data from LdRS (Anderson et al., 2011), (F) arboreal pollen (AP) data from Padul-15-05 (Ramos-Román et al., 2018), and (G) 37°N summer insolation (Laskar et al., 2004). IRHP, DA, MCA, LIA and MCW stand for Iberian Roman Humid Period, Dark Ages, Medieval Climate Anomaly, Little Ice Age and Modern Climate Warming. Red shading indicates warmest summer temperatures in LdRS.

4.5. Pollen-inferred temperature results

The pollen-based summer temperature reconstruction for the last 12,000 cal yr BP shows values oscillating between 9 °C and 13.7 °C (Fig. 8). The increasing temperature trend occurs during the EH, reaching the Holocene maxima of 13.7 °C at 6800 cal yr BP, with average summer temperature values of 12.1 °C between 7700 and 6300 cal yr BP. A temperature decrease of ~1 °C is observed between 6300 and 5600 cal yr BP (average value of 11.2 °C), reaching a minimum temperature of 10.5 °C. Although temperature increases again to above 12 °C at ~5500 cal yr BP, a decreasing trend characterized the end of the MH and the LH, with three minima of 9.9, 9.6 and 9 °C at ~3000, 2000 and 100 cal yr BP, respectively. An increase of more than 2 °C occurred after 1850 CE (100 cal yr BP), reaching values of ~11.4 °C during the last century, indicating temperatures similar or higher than the average recorded during the warmest Holocene period mentioned above (7700-6300 cal yr BP).

5. Discussion

The modern, present-day distribution of chironomid assemblages identified in different altitude-distributed lakes has been shown to be strongly related to the mean summer air and summer surface water temperatures (Heiri et al., 2011; Eggermont and Heiri, 2012). In high-altitude lakes most biological activity, and also the emergence of adult chironomids, takes place in the summer months when the lakes are ice-free (e.g. Walker, 2001). Therefore, fossil chironomid records can provide detailed information on past chironomid assemblage changes, and indirectly also on past temperature conditions.

Fossil chironomid assemblages in lake records have been proven to be sensitive to climate changes, especially in summer air and water temperature, during the late glacial and present interglacial (Heiri et al., 2014; Ilyashuk et al., 2011; Bolland et al., 2020). The PCA run on our fossil chironomid data indicates that temperature is the main environmental factor controlling the chironomid assemblage changes in LdRS. This is deduced from the clear negative correlation of *Micropsectra radialis* type, a cold chironomid species at present (Heiri et al., 2011), and the positive correlation of warmer indicators such as *Psectrocladius sordidellus* type and *Corynoneura arctica* type, to PC1 (Fig. 5). Changes in chironomid assemblages could also be due to hydrological changes such as lake level (Bolland et al., 2021). However, the small size and water depth of the LdRS (see above) and the short sedimentary record (~150 cm long) imply that the variations in lake level, even though previously noted by Anderson et al. (2011), were in the order of maximum 1 m, and unlikely to produce significant changes in the chironomid associations or affect the chironomid-based temperature reconstruction. This is confirmed by the absence or extremely sporadic abundance (e.g., *Metriocnemus*) of chironomid taxa typical for very shallow or semiterrestrial environments and by the good preservation of chitinous remains, which indicates that the lake remained an open water, limnic environment during its entire existence. Both LdRS-06-01 and RS cores studied here were taken from approximately the same location and depth (i.e., the depocenter of the lake: Anderson et al., 2011; Jiménez et al., 2019) and thus the chironomid changes observed are not due to environmental differences, such as depth, in the location of the two cores. Changes in productivity and/or the amount of dissolved oxygen also play a role in conditioning certain chironomid assemblages, such as the occurrence and abundance of *Chironomus* species, in present-day lakes (e.g., Raposeiro et al., 2018). However, a previous study from the studied LdRS-06-01 core shows that the peak in organic content (TOC) and thus productivity at 5500 cal yr BP (Jiménez-Espejo et al., 2014) occurred asynchronously with the maximum occurrence of *C. plumosus* at 7800 cal yr BP, suggesting little or no relationship. These studies also show no evidence of major changes in the lake water oxygenation at LdRS (Anderson et al., 2011; Jiménez-Espejo et al., 2014; García-Alix et al., 2013, 2018).

The chironomid-based temperature reconstruction relies on a calibration dataset that documents the range of chironomid assemblage compositions that are found under varying environmental and particular temperature conditions. Based on these calibration data numerical models, e.g., based on weighted averaging partial least squares (WA-PLS) or maximum likelihood regression (e.g., Brooks and Birks, 2001; Heiri et al., 2011) are then developed that predict the most likely temperature conditions for a particular chironomid assemblage observed in a sediment record. For Europe a number of regional chironomid-temperature calibration datasets have been developed, e.g., from Finland (Luoto, 2009), northern Sweden (Larocque et al., 2001), Norway (Brooks and Birks, 2001) or Switzerland (Heiri and Lotter, 2010). However, for southern European mountain regions no dedicated, local chironomid-temperature calibration dataset is presently available. For our reconstruction, we relied on the joined 274-lake chironomid-temperature calibration dataset and transfer function from the Swiss Alps and Norway. The dataset covers a wide range of altitudes and temperature conditions in both Norway and the Swiss Alps and has been successfully applied to southern European mountain lakes for temperature reconstruction (Samartin et al., 2017; Tarrats et al., 2018; Jiménez et al., 2019). All the morphotypes found in LdRS are well represented in these data and particularly in samples from high-altitude lakes in the Alps.

Comparisons of individual geophysical, vegetation and chironomid curves show similar changes in the LdRS record (Fig. 6). For example, the deglaciation (Late Pleistocene and earliest Holocene) section of the record is characterized by high MS values, high *Artemisia* percentages and high values in *M. radialis*-type, a cold indicating chironomid taxon. At the Pleistocene-to-Holocene transition all three curves show abrupt changes, showing that changes in the lake catchment and lake ecosystem were closely coupled. Similarly, *Artemisia* and *M. radialis*-type show synchronous increases in the LH, indicating synchronous climate impacts on lake catchment and LdRS during the past millennia.

5.1. Late Pleistocene coldest maxima

Based on the LdRS record, the coldest conditions occurred during the last glacial maximum and deglaciation between ~21,000 and 13,000 cal yr BP in the Sierra Nevada. This is indicated by the coldest chironomid-inferred July air temperature reconstruction around 6 °C (4.5–7.5 °C) (Fig. 7), largely a consequence of the highest abundances of *Micropsectra radialis* type in five samples studied from the lowermost part of the LdRS record (Figs. 3 and 6). *M. radialis* is dominant in the coldest lakes in the Alps and Norway (Heiri et al., 2011), occurring commonly above 2000 m in Spain (Rieradevall et al., 1999). Coldest conditions were possibly related to summer insolation minima at that time (Laskar et al., 2004, Fig. 7) generating generally cold, ice-age conditions that characterized the North Atlantic and adjacent regions (Clark et al., 2012). *Micropsectra radialis* type is leading to the coldest reconstructed temperatures of the Late Pleistocene. Cold conditions

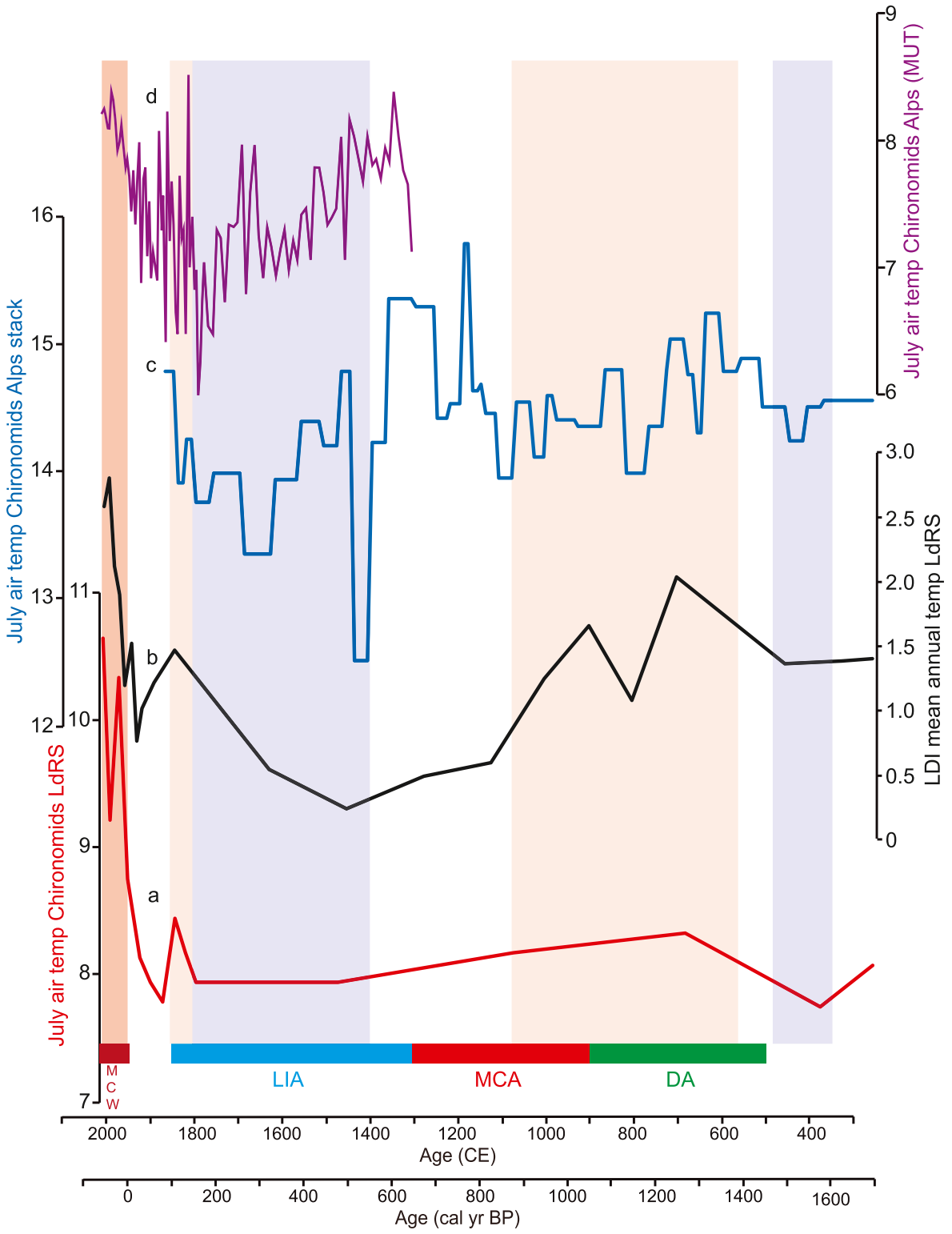

Fig. 9. Comparison of the (A) chironomid-inferred July air temperature from LdRS for the last 1700 cal yr BP with (B) the LDI mean annual temperature reconstruction from LdRS (García-Alix et al., 2020), (C) a stacked and spliced July air temperature reconstruction from the Alps based on chironomids (Heiri and Lotter, 2005) and (D) the Mutterbergersee Lake (MUT; Eastern Alps) (Ilyashuk et al., 2019). DA, MCA, LIA and MCW stand for Dark Ages, Medieval Climate Anomaly, Little Ice Age and Modern Climate Warming. Red shadings highlight warm periods in LdRS. Blue shadings indicate cold periods recorded in LdRS.

within the lake basin could have also been amplified due to the influence of cold melt-water from LGM or YD glacial melting, as this may have led to lower temperatures than expected due to ambient air temperatures. The low number of chironomid capsules occurring in the sediments deposited during this time of very low sedimentary rates could also be explained by the low temperatures that probably reduced the biological activity in the lake in this period. Coldest conditions are also deduced by the abundance of the steppe-like vegetation dominated by *Artemisia* in the area and high, possibly glacier-derived, detritic sedimentation (and thus high MS) in the LdRS lake (Fig. 6; Anderson et al., 2011). Harsh

environmental and climate conditions were also registered in the sediments from Laguna Seca, another alpine lake from Sierra Nevada. López-Avilés et al. (2022) interpreted the sedimentary facies recorded between 17,700 and 15,700 cal yr BP as glaciogenic deposits (till) or nivation sediments product of seasonal climate oscillations under very cold and arid conditions. At the Sierra Nevada, glacier maximum advance occurred during the last glaciation, followed by a massive deglaciation at ~20,000–19,000 yr, until a new glacier advance occurred during HS1 (Palacios et al., 2016). After HS1 a probable almost total disappearance of the glaciers took place and only small cirque glaciers formed during the Younger Dryas (Palacios et al., 2020). Mean annual air temperatures (MAAT) based on the distribution of specific bacterial membrane lipids, known as brGDGTs, have shown minimum values of 12 °C during the Heinrich Stadial 1 (HS1) in the Padul record, a low elevation paleolake in Sierra Nevada (Rodrigo-Gámiz et al., 2022). Differences in absolute temperature values, which are in order of ~6° higher in Padul than in LdRS records, are expected due to the difference in elevation (more than 2000 m between the two sites) and the different biological sources to infer air temperatures. Marine records also registered the lowest sea surface temperatures (SST) of the last 22,000 yr during the last deglaciation, especially during the Heinrich stadial 1 (18, 000–14,900 cal yr BP) with SST ~6 °C in the South Iberian Atlantic margin (Sierro et al., 2020) and 6 to 10 °C, depending of the used proxy in the South Iberian Mediterranean margin (Morcillo-Montalbá et al., 2021).

Our study also updates the chronology of the previous works done on the LdRS sedimentary record. Previously, no radiocarbon dates beyond 9540 cal yr BP were obtained (Fig. 2; Table 1), leading to a relatively poor age control for the organic-poor lowermost part of the sedimentary record. As a consequence, previous studies from LdRS interpret this part showing high percentages of *Artemisia* and other steppic and cold indicators as the transition from Younger Dryas (YD) to EH or earliest Holocene (Anderson et al., 2011; García-Alix et al., 2013, 2018, 2020; Jiménez-Espejo et al., 2014; Jiménez et al., 2018, 2019; Toney et al., 2020). Our new age data and the chironomid assemblages show that the bottommost part of the LdRS sedimentary record could have been deposited during very cold conditions and related to the end of the last glaciation, the LGM, or last deglaciation cold periods HS1 or YD (Figs. 6 and 7).

5.2. Holocene thermal maximum (HTM): Timing and warming amplitude

Based on the chironomid record, summer temperature warming occurred in the LdRS in the latest Pleistocene and EH, with an estimated warming rate of ~6 °C, from ~4.5 to 10.5 °C from ~13,000–8600 cal yr BP (Figs. 7 and 8). Based on our new radiocarbon dates the timing of this warming now seems to be later than expected based on earlier studies (Anderson et al., 2011; García-Alix et al., 2013, 2018; Jiménez-Espejo et al., 2014). However, the age of this section of the record is mainly constrained by a single radiocarbon date (9481 cal yr BP) at 134 cm depth (Table 1) and the ages of this section of the sediment record should be interpreted with caution. Irrespective of the exact age of this transition, the increase in summer temperatures is represented by an increase in the total number of head capsules (Fig. 4) together with a distinct change in the chironomid assemblages. Notably, there is a decrease in *Micropsectra radialis* type and an increase in warmer adapted taxa such as *Chironomus plumosus* type, *Chironomus anthracinus* type, *Heterotrissocladius marcidus* type, *Metriocnemus* and taxa with a broader temperature distribution such as *Psectrocladius sordidellus type* and *Corynoneura arctica* type (Heiri et al., 2011). Particularly head capsules of *Chironomus plumosus* type are rarely found in high-elevation lakes. For example, in the Alps they are restricted to July temperatures above 10 °C. Warming generated the disappearance of glaciers of the studied massif at that time (Oliva et al., 2020) and was associated with significant vegetation changes with the increase in mesic tree forest species (represented by AP in Fig. 8) such as *Pinus*, deciduous *Quercus* or *Betula* in the Sierra Nevada area (Anderson et al., 2011).

The LdRS chironomid summer temperature reconstruction shows that the HTM is recorded during the EH and early MH between ~9000 and 7200 cal yr BP, although the earliest part of the Holocene is again less well constrained by radiocarbon ages than later sections and the MH to LH. July temperature estimations based on chironomids are above 10 °C and a maximum peak of 10.8 °C at ~7250 cal yr BP, more than two degrees higher than preindustrial times (e.g., 1850 CE) (Figs. 7–9). In a recent reconstruction of global mean surface temperatures (GMST), the highest temperatures of the Holocene were inferred to be at ~6500 cal yr BP, which were ~0.6 °C warmer than the 1800–1900 CE reference period (Kaufman et al., 2020a, 2020b), although this study represents mean annual rather than summer temperatures. With respect to the timing of the HTM, the only chironomid-inferred summer temperature record from Spain, the Basa de la Mora Lake record at lower elevation than LdRS (1914 m a.s.l.), also shows a later HTM between 8000 and 6000 cal yr BP (Tarrats et al., 2018), similar to chironomid-based temperature reconstructions based on chironomid records from the Italian Apennines (Lago Gemini inferiore: 1349 m a.s.l. and Lago Verdarolo: 1390 m a.s.l.; Samartin et al., 2017). Irrespective of the EH dating uncertainties, our study suggests that the HTM was reached earlier at LdRS with a relatively higher amplitude of temperature change. Our study agrees with a chironomid-based temperature reconstruction from a high-altitude lake in the Alps, Schwarzsee ob Sölden (Tyrol, Austria), which also shows an HTM prior to 8000 cal yr BP and between 9500 and 9000 cal yr BP (Ilyashuk et al., 2011), suggesting some regional variation in respect to the timing of the HTM across European sites. A reconstruction based on climate model of intermediate complexity shows a HTM between 8000 and 5000 cal yr BP in Europe (Renssen et al., 2009). However, that study also shows that the timing and magnitude of the HTM vary depending on the location, confirming that besides insolation there are other major forcings and feedbacks controlling climate at a certain site such as albedo, topography, the persistence of ice sheets such as the Fennonscandian and Laurentide ice sheets into the Holocene (persisting until ~9000 and 7000-6000 cal yr BP respectively) and ocean heat transport, a finding supported by various proxy records. For example, many studies in North America and the North Atlantic show a delay in the HTM with respect to summer insolation mostly related to the influence of the Laurentide Ice Sheet and its disappearance around 7000-6000 cal yr BP from North America (Kaufman et al., 2004; Renssen et al., 2009). Although the LdRS chironomid-based temperature record shows a delayed warming in the EH (with the limitation of the poor age control for this part of the record), it does not resemble the temperature development expected for sites influenced by the lingering effects of the Laurentide Ice Sheet dynamics and instead represents changes expected for locations predominantly conditioned by orbital-induced summer insolation (Fig. 8). Rapid warming and melting of glaciers in the Sierra Nevada in the EH facilitated the expansion of forest towards higher elevation and tundra-like vegetation in alpine areas (Anderson et al., 2011), most-likely reducing surface albedo and producing a positive temperature feedback in-phase with summer insolation. The effect of elevation and/or latitude on climate could account for some of the differences in the timing of HTM in the European chironomid-inferred temperature records. This is supported by the observation that a chironomid-based temperature record from a high-elevation site from the Austrian Alps (Schwarzsee ob Sölden at 2796 m a.s.l.) resembles the LdRS (3029 m a.s.l.) temperature features and shows a relatively early HTM during the EH between 10,000 and 8600 cal yr BP followed by a temperature decrease (Ilyashuk et al., 2011). However, a chironomid-based summer temperature stack from the Alps shows a more prolonged HTM, from 9200 to 4700 cal yr BP during the EH and MH (Heiri and Lotter, 2005, Fig. 8), with temperatures only decreasing later, indicating differences also in the duration of the HTM. Paleoclimatic disparities over the elevational gradient were also previously suggested for the Sierra Nevada based on asynchronicities in the timing of the Holocene mesophytic maximum

(combining temperature and precipitation) in pollen records from high-elevation alpine sites from the Sierra Nevada and the Holocene mesophytic maximum deduced from lower elevation paleoclimatic sites from the same region (Anderson et al., 2011). The earlier timing of the mesophytic maximum during the EH in the higher elevation Sierra Nevada area was explained by maxima in seasonality, which generated greater snowpack in winter that translated into overall more humidity throughout the year and higher lake levels, while in adjacent lowlands highest summer insolation produced warmer temperatures during summer, generating higher evaporation and evapotranspiration and less humidity than at higher elevations (Anderson et al., 2011; Ramos-Román et al., 2018). The timing of the HTM and particularly the early decrease of the maximum temperatures at LdRS seems to resemble more the GMST dynamics in northern high latitudes (60-90°N) forced principally by summer insolation (Kaufman et al., 2020a, 2020b). Climate changes are also amplified in polar (high-latitude) and alpine (high-altitude) regions (IPCC et al., 2022), probably due to the fast reduction in surface albedo, generating a positive temperature feedback in-phase with summer insolation.

The comparison of the chironomid-inferred July temperature estimations with the previously published pollen data from LdRS and our new summer temperature estimations obtained from the LdRS pollen data show differences in timing between the HTM in the temperature record and the Holocene maximum in arboreal pollen (Fig. 8), a pollen category often interpreted as indicating maximum temperatures in pollen records, particularly at high-latitude and high-altitude sites. Summer temperatures reconstructed from the pollen data also suggest a mid-Holocene summer temperature maximum like the chironomid data, but with maximum values ca. 1500 years later and relatively warm temperatures lasting until ca. 4500 cal yr BP. In contrast chironomid inferred temperatures already decrease from ca. 7000 cal yr BP onwards. However, in the Mediterranean region, vegetation responds to temperatures but also to changes in precipitation and evapotranspiration (Jiménez-Moreno and Anderson, 2012; Samartin et al., 2017; Kaufman et al., 2020a, 2020b). The delay and prolonged climatic optimum for trees shown by arboreal pollen data from LdRS and Padul and the LdRS pollen temperature estimations (Fig. 8) could be explained by the response of the vegetation to reducing summer insolation during the MH and thus reduction in evapotranspiration that could have favored enhanced humidity and the later development and persistence of tree species such as deciduous *Quercus*, *Betula* or pine trees in the area.

In the LdRS chironomid record, the HTM is interrupted by a short-term minimum in temperature of ~9.2 °C at ~7350 cal yr BP. The MAAT temperature reconstruction based on brGDGTs from the Padul-15-05 sedimentary core also recorded a minimum temperature value of 13 °C at around 7400 cal yr BP (Rodrigo-Gámiz et al., 2022). This agrees with a forest reduction at that time also recorded in the same Padul record (Ramos-Román et al., 2018, Fig. 8), pointing to a regional temperature feature. Reduced summer temperatures have also been described in southern Europe (i.e., Joannin et al., 2012), northern Fennoscandia at ~7200 cal yr BP (Korhola et al., 2000) and N Poland at ~7500 cal yr BP (Pędziszewska et al., 2015) and westernmost Mediterranean SST (Jiménez-Espejo et al., 2008; Morcillo-Montalbá et al., 2021), and recent studies point to an almost global cold event at this time (Hou et al., 2023). Ice-rafted debris events in the North Atlantic occurred at ~7500 cal yr BP indicating cold conditions in the North Atlantic area (Bond et al., 1997). Perhaps the cold event recorded in LdRS was related to a regional Northern Hemisphere feature in climate that could have also caused a cooling in the North Atlantic, (e.g., a glacial lake outburst in the drainage area of the Lake-Agassiz-Obijway as described by Carlson et al. (2008) in the interval 7500–7000 cal yr BP), but it remains uncertain due to relatively low sampling resolution and the dating uncertainties of our record.

5.3. Middle and Late Holocene cooling

Rapid cooling of ~1.5 °C occurred in the chironomid-inferred temperatures after the HTM and between ~7200 and 6500 cal yr BP and was associated with a change in the chironomid assemblages with the decrease in some thermophilous taxa (see above) and the increase in *Psectrocladius sordidellus* type (Figs. 4 and 7). This cooling deduced by the chironomid record coincided in time with the highest summer temperature reconstructions deduced by the pollen (Fig. 8). This shows a delayed maximum temperature for the pollen estimations with respect to the chironomids, which could have been produced by a bias in the pollen record induced by the increase in soil humidity as indicated above. Another explanation for this difference might be the different meaning of the paleoclimatic signal, more regional for pollen and local for chironomids.

Our reconstruction shows a progressive cooling of more than two-degree Celsius during the MH and LH, a trend which also agrees with reconstructions of the global mean surface temperature (Kaufman et al., 2020a, Fig. 8) but particularly also with other qualitative and quantitative temperature records from southern Europe. For example, a similar 1.5 °C cooling was observed in the Pyrenees but starting later on at 6000 cal yr BP (Tarrats et al., 2018) with similar decreases recorded in other chironomid-based temperature reconstructions from Central and southern European mountain ranges (e.g., Heiri et al. 2015; Toth et al., 2015; Samartin et al., 2017). This decrease in summer temperatures was probably related to a progressive orbitally triggered Northern Hemisphere reduction in summer insolation in the MH and LH (Laskar et al., 2004, Fig. 8). This cooling, together with an aridification process generated by the decrease in winter precipitation, likely produced the decrease in forest vegetation in the study area observed in the last millennia (Anderson et al., 2011; Jiménez-Moreno and Anderson, 2012; Ramos-Román et al., 2016, 2018; Mesa-Fernández et al., 2018; García-Alix et al., 2021; Jiménez-Moreno et al., 2022).

Chironomid-estimated summer temperatures from LdRS show a plateau between ~6500 and 3000 cal yr BP (Fig. 8). A similar temperature plateau though with some variability was also noticed between 7000 and 3000 cal yr BP in the Austrian Alps (Ilyashuk et al., 2011), perhaps pointing to a common feature in the European summer temperature evolution at high elevation sites.

Our study shows that further cooling occurred during the LH. This is indicated by the increase in *M. radialis* type that reflects a progressive cooling in the chironomid fauna (Figs. 4 and 6). A cold event apparently occurred at ~2700 cal yr BP, which produced a change in the chironomid association with the peak in *M. radialis* type, a reduction in forest species in the area (Anderson et al., 2011; Jiménez-Moreno et al., 2022, Figs. 6 and 8) and the development of small glaciers in the northern cirques in the Sierra Nevada between 2800 and 2700 cal yr BP (Oliva et al., 2020). The resolution of the chironomid record is not sufficient to provide details about the duration or the centennial scale amplitude of this event. However, a short-term, decadal to centennial-scale solar minimum and associated climatic changes have been reported for Europe around this time (Martín-Puertas et al., 2012). These changes coincided with a cooling centered at 2700 cal yr BP recorded in North Atlantic sediments (Bond et al., 1997) and the temperature decrease at LdRS may possibly be related to this event. Slightly warmer conditions occurred between 2200 and 1700 cal yr BP, mostly coincident with the well-known Iberian Roman Humid Period (IRHP, 2600-1600 cal yr BP; Martín-Puertas et al., 2009), agreeing with regional records also showing slightly warmer and more humid conditions around that time (Jiménez-Moreno et al., 2013; López-Avilés et al., 2021). Higher development of forest vegetation (fuel) together with higher temperatures triggered an increase in forest fires in the Sierra Nevada area during the IRHP (Jiménez-Moreno et al., 2013; Ramos-Román et al., 2016).

Summer temperature variations in our chironomid-based record are relatively minor during the last two millennia and well within the

prediction error of the model (Figs. 7 and 9). However, the timing of these minor variations agrees well with expected temperature changes for this period, with two temperature minima of 7.7 °C around 1550 cal yr BP (~400 CE) and 7.9 °C at ~200 cal yr BP (~1750 CE), at the beginning of the Dark Ages (DA) and Little Ice Age (LIA), respectively (Figs. 8 and 9). A slight warming is apparent at around 1250-1000 cal yr BP during the DA and Medieval Climate Anomaly (MCA) with an estimated increase in temperature up to 8.3 °C (Figs. 8 and 9). Again, the resolution of our record is not sufficient to determine the exact timing and duration of these temperature variations. However, it agrees with other results indicating that relatively warm conditions characterized the MCA in the Iberian Peninsula (Moreno et al., 2012), confirmed in the Sierra Nevada by the long chain diol index (LDI)-derived temperature record (García-Alix et al., 2020, Fig. 9b). Relatively cold values characterizing our summer temperature record between 1500 and 1800 CE (Fig. 9), with a minimum around 1750–1800 CE, also agree with regional temperature reconstructions during the LIA (1500–1850 CE) (Moreno et al., 2012). Cold conditions during the LIA, particularly during summer, allowed glacier advances in the main mountain areas in the Iberian Peninsula such as in the Pyrenees and Picos de Europa (González Trueba et al., 2008). In the Sierra Nevada, there is also evidence of glaciers reappearing again during the LIA in locations above 2950 m a.s.l. such as the Mulhacén and Veleta cirques (Oliva and Gómez-Ortiz, 2012; Oliva et al., 2020). Coldest conditions during the LIA between 1750 and 1800 CE are also registered in other chironomid-deduced summer air temperature records, such as the stack from the Alps between 1400 and 1800 CE (Heiri and Lotter, 2005, Fig. 9c) or the chironomid record from Schwarzsee ob Sölden from the Eastern Alps (Ilyashuk et al., 2019, Fig. 9d), which points to a wider regional pattern in temperature dynamics.

A brief warming seems to have occurred in the Sierra Nevada between 1800 and 1840 CE. Our summer air temperature reconstruction records a peak of 8.4 °C around 1840 CE, agreeing with warming recorded with the independent LDI mean annual temperature reconstruction from LdRS (this study and García-Alix et al., 2020, Fig. 9). Glaciers shrunk at this time due to warming and the Mulhacén glacier disappeared between the 18th and 19th centuries (Oliva and Gómez-Ortiz, 2012; Oliva et al., 2020). This warming is also reflected in the high-resolution chironomid-inferred summer temperature record from the high-elevation Austrian Alps (Ilyashuk et al., 2019). A minimum in reconstructed summer air temperatures of 7.8 °C occurred again around 1870 CE, which also agrees with the mean annual temperature reconstruction based on LDI data from LdRS (García-Alix et al., 2020). In summary, although the temporal resolution of our chironomid record is limited in the latest Holocene and reconstructed temperature variations are well within the errors of the applied inference model, local maxima and minima agree surprisingly well with known local and European climate events (e.g., MCA, LIA) and the independent temperature reconstruction from LdRS based on LDI data, indicating an exceptional sensitivity of chironomid assemblages in this lake to past climatic change.

5.4. Modern climate warming (MCW)

Chironomid-estimated summer temperatures increased more than 2 °C from 7.8 to 10.6 °C from 1870 CE to the present, especially since 1950 CE (from 8.7 to 10.6 °C). Such a fast-warming rate is unusual in the LdRS chironomid-inferred temperature record and its amplitude is only comparable to the temperature evolution during the last deglaciation and the early Holocene before the HTM (see above; Fig. 7). A similar steep rate of warming during the MCW was also obtained by the mean annual temperature estimation based on the LDI record from LdRS (García-Alix et al., 2020, Fig. 9), confirming that the extreme warming rate observed at LdRS is not proxy dependent. The more than two-degree warming rate estimated from LdRS during the MCW is higher than the 1 °C temperature warming estimated by GMST between the past decade (2011–2019) and 1850–1900 CE (Kaufman et al., 2020a), suggesting that the recent warming at LdRS is exceptional compared with the mean annual temperature increase during this period. However, Kaufman et al. (2020a) argue that relatively minor warming depicted in their GMST reconstruction during the MCW could have been due to a bias towards cooler temperatures caused by poor recovery of the topmost part of the aquatic environment sedimentary sequences rich in water content. Chironomid-inferred July air temperatures for MCW at the LdRS record are in the same order of magnitude as the GMST increase projected for the rest of this century and beyond of 1.5–2 °C (IPCC et al., 2022), and exceed the goal of limiting global warming in the near term (2021–2040 CE) to 1.5 °C, a threshold which is considered to present multiple risks to ecosystems and humans (IPPC, 2022). Although global mean temperature development can only be compared to a limited extent with temperature amplitudes recorded at an individual site, such as LdRS, these comparisons do show that the recorded MCW temperature increase was major in the Sierra Nevada and of a sufficient amplitude to cause major changes in the natural landscape and ecosystems. A recent study shows enhanced warming during the MCW at higher elevations compared with lowlands (Pepin et al., 2022). Snow-albedo feedback, enhancing warming where snow is decreasing, seems to be the main mechanism responsible for such rapid temperature increases in alpine areas (Pepin and Lundquist, 2008; Scherrer et al., 2012). This process could have been further amplified due to the increase in black carbon or Saharan dust deposition in alpine mountain areas in the last decades (Mesa-Fernández et al., 2018; García-Alix et al., 2020; López-Avilés et al., 2021), particularly in the Sierra Nevada which is exceptionally susceptible to dust transport from the Sahara (Jiménez-Espejo et al., 2014). The IPCC et al. (2022) also shows that warming greater than the global annual average is occurring in many continental regions such as the Arctic. They also show that warming is generally higher over land than over the ocean. Our study confirms that climate change is accelerating in the high mountain areas of the Sierra Nevada and will have profound environmental impacts in these extremely sensitive environments. Marine proxy and instrumental data in the western Mediterranean show a SST rise of ~2.2 °C during the 20th century (Sicre et al., 2016) and Mediterranean outflow bottom waters also indicate warming trends of 0.33 °C/decade in the 21st century (García-Lafuente et al., 2021). In this sense, a warming 3 times faster than the global average has also been observed in the Mediterranean Sea waters during recent decades, likely due to its enclosed nature (Vargas-Yáñez et al., 2010).

A maximum in summer temperatures around 10.6 °C inferred for the MCW is only slightly lower than the estimations obtained during the HTM of 10.8 °C (Fig. 8), confirming that summer temperatures at LdRS are close to their Holocene maximum values and future warming will therefore clearly exceed these. This indicates that at local scales Holocene maximum values are or will soon be exceeded in southwestern Europe, an interpretation that has also been suggested – for very different spatial scales and for mean rather than seasonal temperatures – based on global GMST reconstructions (Kaufman et al., 2020a). Small glaciers that occurred during the LIA and persisted later under critical conditions have shrunk and now disappeared, agreeing with the last historical written mention of glaciers in the Sierra Nevada during the mid-20th century (Oliva and Gómez-Ortiz, 2012; Oliva et al., 2020).

Few temperature reconstructions from lake sedimentary records from Europe show such a distinct temperature increase during the MCW (e.g., Ilyashuk et al., 2019). This is most-likely due to the strong imprint by anthropogenic activities (e.g., pasturing, fish introductions, hydrological modifications) on many European lakes, especially at low elevations, which have distorted the relationship between chironomid assemblage composition and summer temperature conditions (e.g., Heiri and Lotter, 2003, 2005; Eggermont and Heiri, 2012). As a consequence, other environmental variables will in many cases have become more important drivers of chironomid assemblage composition. In this respect, the LdRS record from the Sierra Nevada, where human impact

was very low, has been shown to be of high value (Anderson et al., 2011; Jiménez et al., 2019; García-Alix et al., 2020; Toney et al., 2020). Similarly, it may also be that hydrological processes (e.g., snow melting, cool groundwater input during summer months) may have counteracted summer warming in hydrologically more complicated catchment basins, whereas LdRS is a very simple basin where summer surface water temperatures can be expected to be closely related to air temperatures. A further reason why similar results are not available for other mountain regions could be that few mountain lakes have been analyzed at high-resolution for chironomids in the uppermost sedimentary layers.

6. Conclusions

This study provides the first detailed Late Pleistocene and Holocene chironomid-inferred summer air temperature reconstruction from the Sierra Nevada, southern Spain and southern Europe. This reconstruction shows minima in summer temperature of the last 21,000 cal yr BP, during the LGM or YD. Temperatures rose significantly by about ~6 °C during the EH and the highest temperatures (the HTM) were reached in the EH and early-MH between ~9000 and 7200 cal yr BP. This contrasts with the GMST reconstructions from the northern hemisphere between 30 and 60°N, and with other summer temperature reconstructions from European mountain regions, which shows a later MH climatic optimum with highest temperatures around 6000 cal yr BP. This is possibly related to the high elevation of the study site at ca. 3000 m a.s.l. and to the impacts of the EH summer insolation maxima and various positive-feedback mechanisms.

A continuous cooling trend is observed during the MH and LH until ~1550 and ~200 cal yr BP (~400 and 1750 CE), corresponding to the beginning of the DA and LIA, when minima in Holocene temperatures were reached in the Sierra Nevada. This resembles locally and for summer temperature the trend that has been reported based on a wide range of proxy records for the GMST reconstruction (Kaufman et al., 2020a), which indicate a decreasing trend from the MH onwards to minimum values in the LIA.

Our study shows warming of higher than two-degrees Celsius during the last decades, showing that temperatures are rising at exceptional rates at high elevations in the Sierra Nevada, and, therefore, in the climatically sensitive high-altitude areas of the western Mediterranean region. Based on our record, the last time when an acute temperature increase was experienced in southwestern Iberia was at the Lateglacial to Holocene transition. Serious consequences are expected for biodiversity and ecosystems in the Sierra Nevada and similar mountain ranges in southern Europe if temperatures continue to increase at this rate in alpine areas.

Author contributions

G.J.-M. designed the study and wrote the paper. G.J.-M. and O.H. analyzed the chironomid data and performed the data processing and statistical analysis. J.C. performed the pollen data processing and statistical analysis. A.G.-A., R.S.A., F.J.J.-E., C.L.-B., L.J., C.P.-M., M.R.-G., and A.L.-A., helped with data interpretation and writing the paper.

Declaration of competing interest

The authors declare that they have no known competing financial interests or personal relationships that could have appeared to influence the work reported in this paper.

Data availability

Data will be made available on request.

Acknowledgements

This study was supported by projects CGL2013-47038-R, CGL2017-85415-R and PID2021-125619OB-C21/C22, funded by the *Ministerio de Ciencia e Innovación* of Spain, the *Agencia Estatal de Investigación* and the *Fondo Europeo de Desarrollo Regional* FEDER MCIN/AEI/10.13039/501100011033/FEDER, UE"; *Junta de Andalucía* I + D + i *Junta de Andalucía* 2020 Retos P-20-00059, UGR-FEDER B-RNM-144-UGR18, UGR-FEDER A-RNM-336-UGR20, Project cofinanced by FEDER and LifeWatch-Eric LifeWatch-2019-10-UGR-01 and the research group RNM-190 (Junta de Andalucía). RSA acknowledges several travel grants from Northern Arizona University to support this work. JC thanks the *Ministerio de Ciencia e Innovación* of Spain for the Juan de la Cierva Formación postdoctoral fellowship. ALA acknowledges the predoctoral fellowship BES-2018-084293 provided by the MCIN/AEI/10.13039/501100011033/. CLB acknowledges the European Union for her Marie Sklodowska-Curie grant agreement number 892487 under Horizon 2020 funds. LJ acknowledges the Ministry of Universities of Spain for her Margarita Salas grant (MS2021-204) financed by the European Union -Next Generation EU funds.

References

Anderson, R.S., Jiménez-Moreno, G., Carrión, J.S., Pérez-Martínez, C., 2011. Holocene vegetation history from Laguna de Río Seco, Sierra Nevada, southern Spain. Quat. Sci. Rev. 30, 1615–1629.

Bennike, O., Colgan, W., Hedenäs, L., Heiri, O., Lemdahl, G., Wiberg-Larsen, P., Ribeiro, S., Pronzato, R., Manconi, R., Bjørk, A.A., 2023. An early Pleistocene interglacial deposit at Pingorsuit, north-west Greenland. Boreas 52, 27–41.

Blaauw, M., Christen, J.A., 2011. Flexible paleoclimate age-depth models using an autoregressive gamma process. Bayesian Anal 6, 457–474.

Bolland, A., Rey, F., Gobet, E., Tinner, W., Heiri, O., 2020. Summer temperature development 18,000-14,000 cal. BP recorded by a new chironomid record from Burgäschisee, Swiss Plateau. Quat. Sci. Rev. 243, 106–484.

Bolland, A., Kern, O.A., Allstadt, F.J., Peteet, D., Koutsodendris, A., Pross, J., Heiri, O., 2021. Summer temperatures during the last glaciation (MIS 5c to MIS 3) inferred from a 50,000-year chironomid record from Furamoos, southern Germany. Quat. Sci. Rev. 264, 107008.

Bond, G., Showers, W., Cheseby, M., Lotti, R., Almasi, P., deMenocal, P., Priore, P., Cullen, H., Hajdas, I., Bonani, G., 1997. A pervasive millennial-scale cycle in North Atlantic Holocene and glacial climates. Sci. 278, 1257–1266.

Brooks, S.J., 2006. Fossil midges (Diptera: Chironomidae) as palaeoclimatic indicators for the Eurasian region. Quat. Sci. Rev. 25, 1894–1910.

Brooks, S.J., Birks, H.J.B., 2001. Chironomid-inferred air temperatures from Lateglacial and Holocene sites in north-west Europe: progress and problems. Quat. Sci. Rev. 20, 1723–1741.

Brooks, S.J., Langdon, P.G., Heiri, O., 2007. The identification and use of Palaearctic Chironomidae larvae in palaeoecology. Quaternary Research Association Technical Guide 10, 1–276.

Carlson, A.E., LeGrande, A.N., Oppo, D.W., Came, R.E., Schmidt, G.A., Anslow, F.S., Licciardi, J.M., Obbink, E.A., 2008. Rapid early Holocene deglaciation of the Laurentide ice sheet. Nat. Geosci. 1, 620–624.

Clark, P.U., Shakun, J.D., Baker, P.A., Bartlein, P.J., Brewer, S., Brook, E., Carlson, A.E., Cheng, H., Kaufman, D.S., Liu, Z., Marchitto, T.M., Mix, A.C., Morrill, C., Otto-Bliesner, B.L., Pahnke, K., Russell, J.M., Whitlock, C., Adkins, J.F., Blois, J.L., Clark, J., Colman, S.M., Curry, W.B., Flower, B.P., Heg, F., Johnson, T.C., Lynch-Stieglitz, J., Markgraf, V., McManus, J., Mitrovica, J.X., Moreno, P.I., Williams, J.W., 2012. Global climate evolution during the last deglaciation. Proc. Natl. Acad. Sci. USA 109, 7140–7141.

Davis, B.A.S., et al., 2020. The Eurasian modern pollen database (EMPD), version 2. Earth Syst. Sci. Data 12, 2423–2445.

Díaz de Federico, A., 1980. Estudio geológico del Complejo de Sierra Nevada en la transversal del Puerto de la Ragua (Cordillera Bética), PhD thesis. Universidad de Granada, Granada, Spain.

Díaz-Poso, A., Lorenzo, N., Royé, D., 2023. Spatio-temporal evolution of heat waves severity and expansion across the Iberian Peninsula and Balearic islands. Environ. Res. 217, 114864.

Eggermont, H., Heiri, O., 2012. The chironomid-temperature relationship: expression in nature and palaeoenvironmental implications. Biol. Rev. 87, 430–456.

Fick, S.E., Hijmans, R.J., 2017. WorldClim 2: new 1-km spatial resolution climate surfaces for global land areas. Int. J. Climatol. 37, 4302–4315.

García-Alix, A., Jimenez-Espejo, F.J., Lozano, J.A., Jiménez-Moreno, G., Martinez-Ruiz, F., García Sanjuán, L., Aranda Jiménez, G., García Alfonso, E., Ruiz-Puertas, G., Anderson, R.S., 2013. Anthropogenic impact and lead pollution throughout the Holocene in southern Iberia. Sci. Total Environ. 449, 451–460.

García-Alix, A., Jiménez-Espejo, F.J., Jiménez-Moreno, G., Toney, J.L., Ramos-Román, M.J., Camuera, J., Anderson, R.S., Delgado Huertas, A., Martínez-Ruiz, Queralt, I., 2018. Holocene geochemical footprint from Semi-arid alpine wetlands in southern Spain. Sci. Data 5, 180024.

García-Alix, A., Toney, J.L., Jiménez-Moreno, G., Pérez-Martínez, C., Jiménez, L., Rodrigo-Gámiz, M., Anderson, R.S., Camuera, J., Jiménez-Espejo, F.J., Peña-Angulo, D., Ramos-Román, M.J., 2020. Algal lipids reveal unprecedent warming rates in alpine areas of SW Europe during the Industrial Period. Clim. Past 16, 245–263.

García-Alix, A., Camuera, J., Ramos-Román, M.J., Toney, J.L., Sachse, D., Schefuß, E., Jiménez-Moreno, G., Jiménez-Espejo, F.J., López-Avilés, A., Anderson, R.S., Yanes, Y., 2021. Paleohydrological dynamics in the Western Mediterranean during the last glacial cycle. Global Planet. Change 202, 103527.

García-Jurado, F., Jiménez-Gómez, F., Guerrero, F., 2011. Effects of a dry period on the limnological characteristics of a Mediterranean high mountain lake. Limnética 30, 5–16.

García-Lafuente, J., Sammartino, S., Huertas, I.E., Flecha, S., Sánchez-Leal, R.F., Naranjo, C., Nadal, I., Bellanco, M.J., 2021. Hotter and weaker Mediterranean outflow as a response to basin-wide alterations. Front. Mar. Sci. 8, 613444.

González Trueba, J.J., Moreno, R.M., Martínez De Pisón, E., Serrano, E., 2008. "Little ice age" glaciation and current glaciers in the Iberian Peninsula. Holocene 18, 551–568.

Grimm, E.C., 1987. CONISS: a Fortran 77 program for stratigraphically constrained cluster analysis by the method of incremental sum of squares. Comput. Geosci. 13, 13–35.

Grimm, E.C., 1992. Tilia, Version 2. Springfield. IL 62703. Illinois State Museum. Research and Collection Center, USA.

Hammer, Ø., Harper, D.A.T., Ryan, P.D., 2001. PAST: Paleontological statistics software package for Education and data analysis. Palaeontol. Electron. 4 (1), 9pp.

Heiri, O., Lotter, A.F., 2003. 9000 years of chironomid assemblage dynamics in an alpine lake: long-term trends, sensitivity to disturbance, and resilience of the fauna. J. Paleolimnol. 30 (3), 273–289.

Heiri, O., Lotter, A.F., 2005. Holocene and Lateglacial summer temperature reconstruction in the Swiss Alps based on fossil assemblages of aquatic organisms: a review. Boreas 34, 506–516.

Heiri, O., Lotter, A.F., 2010. How does taxonomic resolution affect chironomid-based temperature reconstruction? J. Paleolimnol. 44, 589–601.

Heiri, O., Brooks, S.J., Birks, H.J.B., Lotter, A.F., 2011. A 274-lake calibration data-set and inference model for chironomid-based summer air temperature reconstruction in Europe. Quat. Sci. Rev. 30, 3445–3456.

Heiri, O., Brooks, S.J., Renssen, H., Bedford, A., Hazekamp, M., Ilyashuk, B., Jeffers, E.S., Lang, B., Kirilova, E., Kuiper, S., Millet, L., Samartin, S., Toth, M., Verbruggen, F., Watson, J.E., van Asch, N., Lammertsma, E., Amon, L., Birks, H.H., Birks, H.J.B., Mortensen, M.F., Hoek, W.Z., Magyari, E., Sobrino, C.M., Seppa, H., Tinner, W., Tonkov, S., Veski, S., Lotter, A.F., 2014. Validation of climate model-inferred regional temperature change for late-glacial Europe. Nature Communications, 2015. In: Heiri, O., Ilyashuk, B., Millet, L., Samartin, S., Lotter, A.F. (Eds.), Stacking of Discontinuous Regional Palaeoclimate Records: Chironomid-Based Summer Temperatures from the Alpine Region, vol. 5, p. 5914. Holocene 25(1), 137-149.

Hou, M., Wu, W., Cohen, D.J., Zeng, Z., Huang, H., Zheng, H., Ge, Q., 2023. Detection of a mid-Holocene climate event at 7.2 ka BP based on an analysis of globally-distributed multi-proxy records. Palaeogeogr. Palaeoclimatol. Palaeoecol. 618, 111525.

Ilyashuk, E.A., Koinig, K.A., Heiri, O., Ilyashuk, B.P., Psenner, R., 2011. Holocene temperature variations at a high-altitude site in the Eastern Alps: a chironomid record from Schwarzsee ob Sölden, Austria. Quat. Sci. Rev. 30, 176–191.

Ilyashuk, E.A., Heiri, O., Ilyashuk, B.P., Koinig, K.A., Psenner, R., 2019. The Little Ice Age signature in a 700-year high-resolution chironomid record of summer temperatures in the Central Eastern Alps. Clim. Dynam. 52, 6953–6967.

IPCC, 2022. In: Pörtner, H.-O., Roberts, D.C., Tignor, M., Poloczanska, E.S., Mintenbeck, K., Alegría, A., Craig, M., Langsdorf, S., Löschke, S., Möller, V., Okem, A., Rama, B. (Eds.), Climate Change 2022: Impacts, Adaptation, and Vulnerability. Contribution of Working Group II to the Sixth Assessment Report of the Intergovernmental Panel on Climate Change. Cambridge University Press.

Jiménez, L., Ruhland, K.M., Jeziorski, A., Smol, J.P., Pérez-Martínez, C., 2018. Climate change and Saharan dust drive recent cladoceran and primary production changes in remote alpine lakes of Sierra Nevada, Spain. Global Change Biol. 28, 139–158.

Jiménez, L., Conde-Porcuna, J.M., García-Alix, A., Toney, J.L., Anderson, R.S., Heiri, O., Pérez-Martínez, C., 2019. Ecosystem responses to climate-related changes in a Mediterranean alpine environment over the last ~ 180 years. Ecosystems 22, 563–577.

Jiménez-Espejo, F.J., Martínez-Ruiz, F., Rogerson, M., González-Donoso, J.M., Romero, O., Linares, D., Sakamoto, T., Gallego-Torres, D., Rueda Ruiz, J.L., Ortega-Huertas, M., Perez Claros, J.A., 2008. Detrital input, productivity fluctuations, and wáter mass circulation in the westernmost Mediterranean Sea since the Last Glacial Maximum. Geochem. Geophy. Geosy. 9, Q11U02.

Jiménez-Espejo, F.J., García-Alix, A., Jiménez-Moreno, G., Martínez-Ruiz, F., Anderson, R.S., Rodríguez-Tovar, F.J., Giralt, S., Rodrigo-Gámiz, M., Delgado Huertas, A., Pardo-Igúzquiza, E., 2014. Saharan aeolian input and effective humidity variations over Western Europe during the Holocene. Chem. Geol. 374–375, 1–12.

Jiménez-Moreno, G., Anderson, R.S., 2012. Holocene vegetation and climate change recorded in alpine bog sediments from the Borreguiles de la Virgen, Sierra Nevada, southern Spain. Quat. Res. 77, 44–53.

Jiménez-Moreno, G., García-Alix, A., Hernández-Corbalán, M.D., Anderson, R.S., Delgado-Huertas, A., 2013. Vegetation, fire, climate and human disturbance history in the southwestern Mediterranean area during the late Holocene. Quat. Res. 79, 110–122.

Jiménez-Moreno, G., García-Alix, A., Anderson, R.S., Ramos-Román, M.J., Camuera, J., Mesa-Fernández, J.M., Toney, J.L., Jiménez-Espejo, F.J., Carrión, J.S., López-Avilés, A., Rodrigo-Gámiz, M., Webster, C.E., 2022. Reconstruction of past environment and climate using Wetland sediment records from the Sierra Nevada. In: Zamora, R., Oliva, M. (Eds.), The Landscape of the Sierra Nevada. Springer Nature Switzerland AG, pp. 95–114.

Joannin, S., Brugiapaglia, E., de Beaulieu, J.-L., Bernardo, L., Magny, M., Peyron, O., Goring, S., Vannière, B., 2012. Pollen-based reconstruction of Holocene vegetation and climate in southern Italy: the case of Lago Trifoglietti. Clim. Past 8, 1973–1996.

Juggins, S., 2007. C2 Version 1.5: Software for Ecological and Palaeoecological Data Analysis and Visualization. Newcastle University, Newcastle upon Tyne, UK.

Kaufman, D.S., Ager, T.A., Anderson, N.J., Anderson, P.M., Andrews, J.T., Bartlein, P.J., Brubaker, L.B., Coats, L.L., Cwynar, L.C., Duvall, M.L., Dyke, A.S., Edwards, M.E., Eisner, W.R., Gajewski, K., Geirsdottir, A., Hu, F.S., Jennings, A.E., Kaplan, M.R., Kerwin, M.N., Lozhkin, A.V., MacDonald, G.M., Miller, G.H., Mock, C.J., Oswald, W. W., Otto-Bliesner, B.L., Porinchu, D.F., Ruhland, K., Smol, J.P., Steig, E.J., Wolfe, B. B., 2004. Holocene thermal maximum in the western Arctic(0-180 degrees W). Quat. Sci. Rev. 23, 529–560.

Kaufman, D., McKay, N., Routson, C., Erb, M., Dätwyler, C., Sommer, P.S., Heiri, O., Davis, B., 2020a. Holocene global mean surface temperature, a multi-method reconstruction approach. Sci. Data 7, 201.

Kaufman, D., McKay, N., Routson, C., Erb, M., Davis, B., Heiri, O., Jaccard, S., Tierney, J., Dätwyler, C., et al., 2020b. A global database of Holocene paleo-temperature records. Sci. Data 7, 115.

Korhola, A., Weckström, J., Holmström, L., Erästö, P., 2000. A quantitative Holocene climatic record from diatoms in northern Fennoscandia. Quat. Res. 54, 284–294.

Larocque, I., Hall, R.I., Grahn, E., 2001. Chironomids as indicators of climate change: a 100-lake training set from a subarctic region of northern Sweden (Lapland). J. Paleolimnol. 26, 307–322.

Laskar, J., Robutel, P., Joutel, F., Gastineau, M., Correia, A.C.M., Levrard, B., 2004. A long-term numerical solution for the insolation quantities of the Earth. Astron. Astrophys. 428, 261–285.

Legendre, P., Birks, H.J.H., 2012. From classical to canonical ordination. In: Birks, H.J.B., Lotter, A.F., Juggins, S., Smol, J.P. (Eds.), Tracking Environmental Change Using Lake Sediments Volume 7. Springer, Dordrecht, The Netherlands.

Lepš, J., Šmilauer, P., 2003. Multivariate Analysis of Ecological Data Using Canoco. Cambridge University Press, Cambridge.

López-Avilés, A., Jiménez-Moreno, G., García-Alix, A., García-García, F., Camuera, J., Anderson, R.S., Sanjurjo-Sánchez, J., Chamorro, C.A., Carrión, J.S., 2022. Post-glacial evolution of alpine environments in the western Mediterranean region: the Laguna Seca record. Catena 211, 106033.

López-Avilés, A., García-Alix, A., Jiménez-Moreno, G., Anderson, R.S., Toney, J.L., Mesa-Fernández, J.M., Jiménez-Espejo, F.J., 2021. Latest Holocene paleoenvironmental and paleoclimate reconstruction from an alpine bog in the Western Mediterranean region: the Borreguil de los Lavaderos de la Reina record (Sierra Nevada). Palaeogeogr. Palaeoclimatol. Palaeoecol. 573, 110434.

Lorenzo, M.N., Alvarez, I., 2022. Future changes of hot extremes in Spain: towards warmer conditions. Nat. Hazards 113, 383–402.

Luoto, T.P., 2009. Subfossil Chironomidae (Insecta: Diptera) along a latitudinal gradient in Finland: development of a new temperature inference model. J. Quat. Sci. 24, 150–158.

Martín-Puertas, C., Valero-Garcés, B.L., Brauer, A., Mata, M.P., Delgado-Huertas, A., Dulski, P., 2009. The Iberian-Roman Humid Period (2600-1600 cal yr BP) in the Zoñar lake varve record (Andalucía, southern Spain). Quat. Res. 71, 108–120.

Martín-Puertas, C., Matthes, K., Brauer, A., Muscheler, A., Hansen, F., Petrick, C., Aldahan, A., Possnert, G., van Geel, B., 2012. Regional atmospheric circulation shifts induced by a grand solar minimum. Nat. Geosci. 5, 397–401.

Mesa-Fernández, J.M., Jiménez-Moreno, G., Rodrigo-Gámiz, M., García-Alix, A., Jiménez-Espejo, F.J., Martínez-Ruiz, F., Scott Anderson, R.S., Camuera, J., Ramos-Román, M.J., 2018. Vegetation and geochemical response to Holocene rapid climate change in the Sierra Nevada (southeastern Iberia): the Laguna Hondera record. Clim. Past 14, 1687–1706.

Morales-Baquero, R., Carrillo, P., Reche, I., Sanchez-Castillo, P., 1999. Nitrogenephosphorus relationship in high mountain lakes: effects of the size of catchment basins. Can. J. Fish. Aquat. Sci. 56, 1809–1817.

Morales-Baquero, R., Conde-Porcuna, J.M., 2000. Effect of the catchment areas on the abundance of zooplankton in high mountain lakes of Sierra Nevada (Spain). Verhandlungen der Internationale Vereinigung für theoretische und angewandte Limnologie 27, 1–5.

Morcillo-Montalbá, L., Rodrigo-Gámiz, M., Martínez-Ruiz, F., Ortega-Huertas, M., Schouten, S., Sinninghe Damsté, J.S., 2021. Rapid climate changes in the westernmost Mediterranean (Alboran Sea) over the last 35 kyr: new insights from four lipid paleothermometers (UK' 37, TEXH 86, RI-OH', and LDI). Paleoceanogr. Paleoclimatol. 36, e2020PA004171.

Moreno, A., Pérez, A., Frigola, J., Nieto-Moreno, V., Rodrigo-Gámiz, M., Martrat, B., González-Sampériz, P., Morellón, M., Martín-Puertas, C., Corella, J.P., Belmonte, Á., Sancho, C., Cacho, I., Herrera, G., Canals, M., Grimalt, J.O., Jiménez-Espejo, F., Martínez-Ruiz, F., Vegas-Vilarrúbia, T., Valero-Garcés, B.L., 2012. The medieval climate Anomaly in the Iberian Peninsula reconstructed from marine and lake records. Quat. Sci. Rev. 43, 16–32, 2012.

Observatorio del cambio, 2020. Global de Sierra Nevada. In: Linaria v1.0. iEcolab e Laboratorio de Ecología Terrestre e Universidad de Granada. http://linaria.obsnev.es.

Oliva, M., Gómez-Ortiz, A., 2012. Late-Holocene environmental dynamics and climate variability in a Mediterranean high mountain environment (Sierra Nevada, Spain) inferred from lake sediments and historical sources. Holocene 22 (8), 915–927.

Oliva, M., Gómez-Ortiz, A., Palacios, D., Salvador-Franch, F., Andrés, N., Tanarro, L.N., Fernández-Fernández, J.M., Barriocanal, C., 2020. Multiproxy reconstruction of Holocene glaciers in Sierra Nevada (south Spain). Medit. Geosci. Rev. 2, 5–19.

PAGES 2k-PMIP3 group, 2015. Continental-scale temperature variability in PMIP3 simulations and PAGES 2k regional temperature reconstructions over the past millennium. Clim. Past 11, 1673–1699.
Palacios, D., Gómez-Ortiz, Andrés, N., Salvador, F., Oliva, M., 2016. Timing and new geomorphologic evidence of the last deglaciation stages in Sierra Nevada (southern Spain). Quat. Sci. Rev. 150, 110–129.
Palacios, D., Oliva, M., Gómez-Ortiz, A., Andrés, N., Fernández-Fernández, J.M., Schimmelpfennig, I., et al., 2020. Climate sensitivity and geomorphological response of cirque glaciers from the late glacial to the Holocene, Sierra Nevada, Spain. Quat. Sci. Rev. 248, 106617.
Pędziszewska, A., Tylmann, W., Witak, M., Piotrowska, N., Maciejewska, E., Latałowa, M., 2015. Holocene environmental changes reflected by pollen, diatoms, and geochemistry of annually laminated sediments of Lake Suminko in the Kashubian Lake District (N Poland). Rev. Palaeobot. Palynol. 216, 55–75.
Pepin, N.C., Lundquist, J.D., 2008. Temperature trends at high elevations: patterns across the globe. Geophys. Res. Lett. 35 (14), L14701.
Pepin, N.C., Arnone, E., Gobiet, A., Haslinger, K., Kotlarski, S., Notarnicola, C., et al., 2022. Climate changes and their elevational patterns in the mountains of the world. Rev. Geophys. 60, e2020RG000730.
Ramos-Román, M.J., Jiménez-Moreno, G., Anderson, R.S., García-Alix, A., Toney, J.L., Jiménez-Espejo, F.J., Carrión, J.S., 2016. Centennial-scale vegetation and North Atlantic oscillation changes during the late Holocene in the western mediterranean. Quat. Sci. Rev. 143, 84–95.
Ramos-Román, M.J., Jiménez-Moreno, G., Camuera, J., García-Alix, A., Anderson, R.S., Jiménez-Espejo, F.J., Sachse, D., Toney, J.L., Carrión, J.S., Webster, C., Yanes, Y., 2018. Millennial-scale cyclical environment and climate variability during the Holocene in the western Mediterranean region deduced from a new multiproxy analysis from the Padul record (Sierra Nevada, Spain). Global Planet. Change 168, 35–53.
Raposeiro, M.P., Saez, A., Giralt, S., Costa, A.C., Gonçalves, V., 2018. Causes of spatial distribution of subfossil diatom and chironomid assemblages in surface sediments of a remote deep island lake. Hydrobiol. (Sofia) 815, 141–163.
Reche, I., Pulido-Villena, E., Morales-Baquero, R., Casamayor, E.O., 2005. Does ecosystem size determine aquatic bacterial richness? Ecology 86, 1715–1722.
Reimer, P., Austin, W., Bard, E., Bayliss, A., Blackwell, P., Bronk Ramsey, C., Talamo, S., 2020. The IntCal20 northern hemisphere radiocarbon age calibration curve (0–55 cal kBP). Radiocarbon 62 (4), 725–757.
Renssen, H., Seppä, H., Heiri, O., Roche, D.M., Goosse, H., Fichetfet, T., 2009. The spatial and temporal complexity of the Holocene thermal maximum. Nature Geosci. 2, 411–414.
Rieradevall, M., Bonada, N., Prat, N., 1999. Substrate and Depth preferencs of macroinvertebrates along a transect in a Pyrenean high mountain lake (Lake Redó, NE Spain). Limnética 17, 127–134.
Rodrigo-Gámiz, M., García-Alix, A., Jiménez-Moreno, G., Ramos-Román, M.J., Camuera, J., Toney, J.L., Sachse, D., Anderson, R.S., Sinninghe Damsté, J.S., 2022. Paleoclimate reconstruction of the last 36 kyr based on branched glycerol dialkyl glycerol tetraethers in the Padul palaeolake record (Sierra Nevada, southern Iberian Peninsula). Quat. Sci. Rev. 281, 107434.
Samartin, S., Heiri, O., Joos, F., Renssen, H., Franke, J., Brönnimann, S., Tinner, W., 2017. Warm Mediterranean mid-Holocene summers inferred from fossil midge assemblages. Nat. Geosci. 10, 207–212.
Sánchez-Castillo, P.M., Cruz-Pizarro, L., Carrillo, P., 1989. Caracterización del fitoplancton de las lagunas de alta montaña de Sierra Nevada (Granada, España) en relación a las características físico-químicas del medio. Limnética 5, 37–50.
Scherrer, S.C., Ceppi, P., Croci-Maspoli, M., Appenzeller, C., 2012. Snow-albedo feedback and Swiss spring temperature trends. Theor. Appl. Climatol. 110 (4), 509–516.
Sicre, M.-A., Jalali, B., Martrat, B., Schmidt, S., Bassetti, M.-A., Kallel, N., 2016. Sea surface temperature variability in the North western mediterranean Sea (Gulf of lion) during the common Era. Earth Planet Sci. Lett. 456, 124–133.
Sierro, F.J., Hodell, D.A., Andersen, N., Azibeiro, L.A., Jimenez-Espejo, F.J., Bahr, A., et al., 2020. Mediterranean overflow over the last 250 kyr: Freshwater forcing from the tropics to the ice sheets. Paleoceanogr. Paleoclimatol. 35, e2020PA003931.
Spanish National Weather Agency, 2022. AEMet Open Data. AEMet Open Data. http://www.aemet.es/es/datos_abiertos/AEMET_OpenData.
Tarrats, P., Heiri, O., Valero-Garcés, B., Cañedo-Argüelles, M., Prat, N., Rieradevall, M., González-Sampériz, P., 2018. Chironomid-inferred Holocene temperature reconstruction in Basa de la Mora Lake (Central Pyrenees). Holocene 28 (11), 1685–1696.
Telford, R.J., Birks, H.J.B., 2005. The secret assumption of transfer functions: problems with spatial autocorrelation in evaluating model performance. Quat. Sci. Rev. 24, 2173–2179.
Ter Braak, C.J.F., Juggins, S., 1993. Weighted averaging partial least squares regression (WA-PLS): an improved method for reconstructing environmental variables from species assemblages. Hydrobiol 269, 485–502.
Ter Braak, C.J.F., Juggins, S., Birks, H.J.B., van der Voet, H., 1993. Weighted averaging partial least squares regression (WA-PLS): definition and comparison with other methods for species-environment calibration. Chapter 25. In: Patil, G.P., Rao, C.R. (Eds.), Multivariate Environmental Statistics, North-Holland, Amsterdam.
Toney, J.L., García-Alix, A., Jiménez-Moreno, G., Anderson, R.S., Moossen, H., Seki, O., 2020. New insights into Holocene hydrology and temperature from lipid biomarkers in western Mediterranean alpine wetlands. Quat. Sci. Rev. 240, 106395.
Toth, M., Magyari, E.K., Buczko, K., Braun, M., Panagiotopoulos, K., Heiri, O., 2015. Chironomid-inferred Holocene temperature changes in the South Carpathians (Romania). Holocene 25 (4), 569–582.
Valle, F., 2003. Mapa de Series de Vegetación de Andalucía. Editorial Rueda, S.L., Madrid.
Vargas-Yáñez, M., Mora, F., García-Martínez, M.C., Tel, E., Zunino, P., Plaza, F., Salat, J., Pascual, J., López-Jurado, J.L., Serra, M., 2010. Climate change in the western Mediterranean Sea 1900-2008. J. Mar. Syst. 82, 171–176.
Walker, I.R., 2001. Midges: Chironomidae and related Diptera. In: Smol, J.P., Birks, H.J.B., Last, W.M. (Eds.), Tracking Environmental Change Using Lake Sediments. Volume 4: Zoological Indicators. Kluwer Academic Publishers, Dordrecht, pp. 43–66.